A&A 408, 465–477 (2003)
DOI: 10.1051/0004-6361:20030714

Astronomy & Astrophysics

A search for Low Surface Brightness galaxies in the near-infrared

III. Nançay H I line observations⋆,⋆⋆

D. Monnier Ragaigne[1], W. van Driel[1], S. E. Schneider[2], C. Balkowski[1], and T. H. Jarrett[3]

[1] Observatoire de Paris, GEPI, CNRS UMR 8111 and Université Paris 7, 5 place Jules Janssen, 92195 Meudon Cedex, France
e-mail: delphine.ragaigne@obspm.fr; chantal.balkowski@obspm.fr
[2] University of Massachusetts, Astronomy Program, 536 LGRC, Amherst, MA 01003, USA
e-mail: schneide@messier.astro.umass.edu
[3] IPAC, Caltech, MS 100-22, 770 South Wilson Av., Pasadena, CA 91125, USA
e-mail: jarrett@ipac.caltech.edu

Received 6 March 2003 / Accepted 12 May 2003

Abstract. A total of 334 Low Surface Brightness galaxies detected in the 2MASS all-sky near-infrared survey have been observed in the 21 cm H I line using the Nançay telescope. All have a K_s-band mean central surface brightness, measured within a 5″ radius, fainter than 18 mag arcsec^{-2} and a K_s-band isophotal radius at the 20 mag arcsec^{-2} level larger than 20″. We present global H I line parameters for the 171 clearly detected objects and the 23 marginal detections, as well as upper limits for the undetected objects. The 171 clear detections comprise 50 previously uncatalogued objects and 41 objects with a PGC entry only.

Key words. galaxies: distances and redshifts – galaxies: general – galaxies: ISM – infrared: galaxies – radio lines: galaxies

1. Introduction

The present paper is part of a series presenting the results of a multi-wavelength (near-infrared, 21-cm H I line and optical) search for Low Surface Brightness (LSB) galaxies using the 2MASS all-sky near-infrared survey. For further details on the sample and other publications in this series, we refer to Monnier Ragaigne et al. (2003a, Paper I). H I line observations made at Arecibo of a sample of a further 367 2MASS candidate LSB galaxies are presented in Paper II (Monnier Ragaigne et al. 2003b).

1.1. Low Surface Brightness galaxies

The brightness of the night sky acts as a filter in the selection of galaxies: when convolved with the true population of galaxies it gives the population of galaxies we observe. In the past few decades, observations of the local universe have shown the existence of LSB galaxies well below the surface brightness of the average previously catalogued galaxies. At present, the LSBs constitute the least well known fraction of galaxies: their number density and physical properties (luminosity, colours, dynamics) are still quite uncertain. This is mainly due to the fundamental difficulty in identifying them in imaging surveys and in measuring their properties. In order to further investigate the properties of the LSB class of galaxies we selected a large sample of them from the 2MASS database, accessing a wavelength domain (the near-infrared) hitherto scarecely explored in the study of LSBs.

There is no unambiguous definition of LSB galaxies, although ones in common use are based on the mean surface brightness within an isophote or within the half-light radius, or on the extrapolated central surface brightness of the disc component alone after carrying out a disc-bulge decomposition. For 2MASS galaxies, we used the mean K_s-band magnitude within a fixed aperture to identify a sample of galaxies with relatively low infrared surface brightnesses. Because galaxies typically have $(B-K) \sim 3.5$–4 (see below) we selected galaxies in which the central surface brightness within a 5″ radius circular aperture was fainter than 18 mag arcsec^{-2} in K_s. This criterion corresponds roughly to the disc-component definition of LSBs which have a blue central surface brightness $\mu_{B_0} > 22.0$ mag arcsec^{-2}.

LSBs have remarkable properties which distinguish them from high surface brightness spirals, notably:

– LSBs seem to constitute at least 50% of the total galaxy population in number in the local Universe, which has strong implications for the faint end slope of the galaxy

Send offprint requests to: W. van Driel,
e-mail: wim.vandriel@obspm.fr

⋆ Tables 3–5 are only available in electronic form at the CDS via anonymous ftp to cdsarc.u-strasbg.fr (130.79.128.5) or via http://cdsweb.u-strasbg.fr/cgi-bin/qcat?J/A+A/408/465

⋆⋆ Figures 1 and 2 are only available in electronic form at http://www.edpsciences.org

luminosity function, on the baryonic matter density and especially on galaxy formation scenarios (O'Neil & Bothun 2000).
– LSBs discs are among the less evolved objects in the local universe since they have a very low star formation rate (van der Hulst et al. 1993; van Zee et al. 1997; van den Hoek et al. 2000).
– LSBs are embedded in dark matter halos which are of lower density and more extended than the haloes around High Surface Brightness (HSB) galaxies, and they are strongly dominated by Dark Matter at all radii (e.g., de Blok et al. 1996; McGaugh et al. 2001).

The star formation history of LSBs has been the subject of recent debate. The LSBs best studied in the optical and in the near-infrared are blue (e.g., Bergvall et al. 1999), indicating a young mean stellar age and/or metallicity. Morphologically, most studied LSBs have discs, but little spiral structure. The current massive star formation rates in LSBs are an order of magnitude lower than those of HSBs (van Zee et al. 1997); H I observations show that LSBs have high gas mass fractions, sometimes exceeding unity (Spitzak & Schneider 1998; McGaugh & de Blok 1997). All these observations are consistent with a scenario in which LSBs are relatively unevolved, low mass surface density, low metallicity systems with roughly constant star formation rate. However, this scenario has difficulty accommodating giant LSBs like Malin 1 (Bothun et al. 1987).

This study of infrared LSBs was also intended to investigate the possibility of the existence of a substantial population of red LSBs, like those reported by O'Neil et al. (1997b). Although the H I study of O'Neil et al. (2000) indicated that some of them did not seem to follow the "standard" Tully-Fisher relation, appearing to be severely underluminous for their total mass, observations by Chung et al. (2002) indicate that their rotational properties were mismeasured due to confusion with neighbouring galaxies. An infrared-selected sample should allow us to identify whether there is a significant population of very red LSBs.

In the present paper results of 21-cm H I line observations made at Nançay is given, wheras a description of the 2MASS LSB galaxy sample selection is given in Paper I, H I observations made at Arecibo are presented in Paper II, optical *BVRI* CCD surface photometry of a sub-sample of 35 galaxies will be presented in Paper IV (Monnier Ragaigne et al. 2003d), an analysis of the full data set will be presented in Paper V in the series, and models of the star formation history of these, and other, samples of LSB galaxies are presented in Boissier et al. (2003).

1.2. The 2MASS all-sky near-infrared survey

The Two Micron All Sky Survey, 2MASS, has imaged the entire celestial sphere in the near-infrared J (1.25 μm), H (1.65 μm) and K_s (2.16 μm) bands from two dedicated, identical 1.3-meter telescopes. The 2MASS data have a 95% completeness level in J, H and K_s of 15.1, 14.3 and 13.5 mag, respectively, for "normal" galaxies (Jarrett et al. 2000; for LSB and blue objects the completeness limits are not yet known). The Extended Source Catalog (XSC) will consist of more than 1.4 million galaxies brighter than 14th mag at K_s with angular diameters greater than $\sim 6''$. The photometry includes accurate PSF-derived measures and a variety of circular and elliptical aperture measures, fully characterizing both point-like and extended objects. The position centroids have an astrometric accuracy better than $\sim 0''.5$. In addition to tabular information, 2MASS archives full-resolution images for each extended object, enabling detailed comparison with other imaging surveys. Initial results for galaxies detected by 2MASS, detailing their properties and detection into the Zone of Avoidance (ZoA), are described in several publications (Schneider et al. 1997; Jarrett et al. 2000a,b; Hurt et al. 2000).

Though relatively less deep than some of the dedicated optical imaging surveys made of LSB galaxies over limited areas of the sky, the 2MASS survey allows the detection of LSBs with a central surface brightness in the K_s band of $\sim$18–20 mag arcsec^{-2}, corresponding to about $\sim$22–24 mag arcsec^{-2} in B, extending over the entire sky. The near-infrared data will be less susceptible than optical surveys to the effects of extinction due to dust, both Galactic and internal to the galaxies.

The selection of the sample of 2MASS near-infrared selected LSB galaxies observed in H I at Nançay is described in Sect. 2, the observations and the data reduction are presented in Sect. 3, and the results in Sect. 4. A brief discussion of the results is given in Sect. 5 and the conclusions are presented in Sect. 6.

2. Sample selection

We have selected 2MASS LSB galaxies using the following two galaxy search routines. For a more complete description of the selection procedures we refer to Paper I. The selected LSB objects lie outside the ZoA ($|b| > 10°$).

• The first is aimed at selecting relatively high signal-to-noise low central surface brightness (LCSB) galaxies, with a mean central K_s surface brightness in the inner $5''$ radius of $K_5 \geq 18$ mag arcsec^{-2}, among the extended sources picked out from the survey data by the standard 2MASS algorithms (Jarrett et al. 2000). All objects observed in H I at Nançay have a 20 mag arcsec^{-2} K_s-band isophotal radius $r_{K_{20}}$ larger than $20''$, i.e., they belong to our sample of "Large" sources (see Paper I).

• The second is aimed at finding lower signal-to-noise LSB galaxies among those sources which were not recognized as such during the standard extended source selection described above. This requires masking all sources detected by the former method and spatially smoothing the remaining data. These sources are referred to as the "Faint" sample, see Paper I.

In order to decide which of these 2MASS sources really are LSB galaxies, additional data were used from online databases such as NED (NASA Extragalactic Database) (`http://nedwww.ipac.caltech.edu`), LEDA (Lyon-Meudon Extragalactic Database) – recently incorporated in HyperLeda (`http://www-obs.univ-lyon1.fr/hypercat/`) – and Aladin of the Centre de Données astronomiques de Strasbourg (CDS)

(http://aladin.u-strasbg.fr), and Digital Sky Survey (DSS) images were inspected. Using this selection procedure, a total of 3800 candidate 2MASS LSB galaxies were found.

The source selection for our survey was made with the 2MASS working database available in late 1999, when work on it was still in full progress. The 229 Large sources we observed at Nançay contain only 12 that are not found in the subsequent, more reliable, 2MASS public data releases (see Paper I for details), 6 of which were detected by us in H I (L125O, L191O, L192O, L270O, L668O and L734O) and 6 that were not (L147N, L328O, L649P, L673O, L761N and L791). Their names have been put in parentheses in the tables. The sample also contains 19 Faint sources, out of the 25 observed at Nançay, that are not found in subsequent public data releases. This high percentage is not surprising, however, considering they were detected by a dedicated LSB galaxy search method and that they were not included in the working database. Thirteen of these were detected (see Table 4) and 6 were not (see Table 7).

Due to constraints in the useable declination range of the instrument, the area of the sky observed at Nançay for our survey ranges from –39° to 60° in declination, and excludes the declination range we observed at Arecibo, i.e. 0° to +39°. Within the chosen area we selected for observation, in order of decreasing priority: (1) all objects with known velocity, and (2) objects without known velocity, whether previously catalogued or not.

3. Observations and data reduction

3.1. Observations

The Nançay decimetric radio telescope, a meridian transit-type instrument of the Kraus/Ohio State design, consists of a fixed spherical mirror (300 m long and 35 m high), a tiltable flat mirror (200 × 40 m), and a focal carriage moving along a curved rail track. Sources on the celestial equator can be tracked for about 60 min. The telescope's collecting area is about 7000 m^2 (equivalent to a 94-m diameter parabolic dish). Due to the E-W elongated shape of the mirrors, some of the instrument's characteristics depend on the declination at which one observes. At 21-cm wavelength the telescope's half-power beam width (HPBW) is 3.′5 in right ascension, independent of declination, while in the North-South direction it is 23′ for declinations up to ∼20°, rising to 25′ at $\delta = 40°$ and to 29′ at $\delta = 60°$, the northern limit of the survey (see also Matthews & van Driel 2000). The instrument's effective collecting area and, consequently, its gain, follow the same geometric effect, decreasing correspondingly with declination. All observations for our project were made after a major renovation of the instrument's focal system (e.g., van Driel et al. 1997), which resulted in a typical system temperature of 35 K.

The observations were made in the period July 2000-June 2002, using a total of about 1500 h of telescope time. We obtained our observations in total power (position-switching) mode using consecutive pairs of 40 s ON and 40 s off-source integrations. Off-source integrations were taken at a position about 20′ E of the target position. Different autocorrelator modes were used for the observation of sources with previously known radial velocities and for velocity searches of objects of unknown redshift.

For objects of known redshift, the autocorrelator was divided into 1 pair of cross-polarized receiver banks, each with 4096 channels and a 25 MHz bandpass, resulting in a channel spacing of 1.3 km s^{-1}. The centre frequencies of the 2 banks were tuned to the redshifted H I line frequency of the target source. These spectra were boxcar smoothed to a channel separation of 17.1 km s^{-1} during the data reduction in order to increase signal-to-noise.

For objects without a known redshift, the autocorrelator was divided into 1 pair of cross-polarized receiver banks, each with 4096 channels and a 50 MHz bandpass, resulting in a channel spacing of 2.6 km s^{-1}. The centre frequencies of the 2 banks were tuned to 5600 km s^{-1}, for a velocity search in the ∼–500 to 10 500 km s^{-1} range (hereafter referred to as a low-velocity search) and to 15 000 km s^{-1}, for a velocity search in the ∼9500 to 20 500 km s^{-1} range for the "high-velocity searches". These spectra were boxcar smoothed to a channel separation of 15.7 km s^{-1} during the data reduction.

Flux calibration, i.e., the conversion of observed system temperatures to flux densities in mJy, is determined for the Nançay telescope through regular measurements of a cold load calibrator and periodic monitoring of strong continuum sources by the Nançay staff. Standard calibration procedures include correction for the abovementioned declination-dependent gain variations of the telescope (e.g., Fouqué et al. 1990). We observed a number of calibrator galaxies throughout our observing runs, see Sect. 5.

3.2. Data reduction

The first steps in the data reduction were made using software developed by the Nançay staff (NAPS, SIR program packages). With this software we averaged the two receiver polarizations, and applied a declination-dependent conversion factor to convert from units of system temperature to flux density in mJy.

Further data analysis was performed using Supermongo routines developed by one of us (SES). With these we subtracted baselines (generally third order polynomials were fitted), excluding those velocity ranges with H I line emission or radio frequency interference (RFI). Once the baselines were subtracted, the radial velocities were corrected to the heliocentric system, according to the conventional optical definition ($V = c(\lambda - \lambda_0)/\lambda_0$) and the central line velocity, line widths at, respectively, the 50% and 20% level of peak maximum (Lewis 1983), the integrated flux of the H I profiles, as well as the rms noise of the spectra were determined. All data were boxcar smoothed to a velocity resolution of 15.7 km s^{-1} (velocity search) and 17.1 km s^{-1} (known velocity) for further analysis.

3.2.1. RFI mitigation

As a consequence of their high sensitivity, radio astronomy telescopes are vulnerable to radio frequency interference (RFI), with signal strengths usually greatly exceeding those of the

weak celestial radio sources being observed. Broad-band RFI raises the noise level of the observations, while narrow-band RFI may mimic spectral lines, like the H I lines from galaxies that were searched for in the present study.

In a regulatory sense, for 21 cm line observations, it should be noted that in the ITU-R Radio Regulations (2001), with which all users of the radio spectrum are obliged to comply, astronomical H I line observations are only protected from "all emissions" out to a redshift of about 4300 km s^{-1}, while for observations out to ~19 000 km s^{-1} "(national frequency) administrations are urged to take all practicable steps to protect the radio astronomy service from harmful interference". These provisions for protection from RFI clearly cannot guarantee a completely interference-free environment for the kind of survey we performed.

At present no universal RFI mitigation method exists for radio astronomy observations (e.g., Fridman & Baan 2001). In order to minimize the effect of RFI in our observations we used an off-line RFI mitigation program, which is part of the standard Nançay NAPS software package. The different steps applied to the individual 40 s integration spectra within a cycle of consecutive spectra of a particular object are as follows:

First, the average of all OFF spectra in the cycle is subtracted from each individual ON spectrum, and then for each resulting individual spectrum the average signal strength and its rms variation is determined, after rejection of 25% of the highest and 25% of the lowest signal strengths. In each individual spectrum the channels with signal strengths deviating by more than $\pm N\sigma$ from the average are flagged, and their signal strengths replaced by a linear interpolation between neighbouring clean channels. The cut-off level was set to 10σ.

Then the average of all cleaned ON spectra in the cycle is subtracted from each individual OFF spectrum. In analogy with the first step, in each resulting individual spectrum the channels with signal strengths exceeding $\pm N\sigma$ from the average are replaced by linear interpolation. This results in cleaned individual OFF spectra.

Finally, the first step is repeated on the individual ON spectra, but this time using the cleaned OFF spectrum resulting from the second step.

Nevertheless, no RFI mitigation technique can simply eliminate all interference (certainly not without the risk of removing part of the line emission that is being searched for), and the detections in the following radial velocity ranges, where the strongest RFI signals occur, should be considered with due care: RFI occurred frequently around 4200, 8250, 12 500 and 17 200 km s^{-1}, regularly around 9000 and 11 700 km s^{-1}, and occasionally around 2000, 9400 and 10 500 km s^{-1}.

4. Results

Our global Nançay H I data for the observed sample, together with their global near-infrared and optical data, are listed in Table 3 for detected objects, in Table 4 for marginal detections and in Table 5 for undetected objects. The H I spectra of the detected galaxies are shown in Fig. 1; for information on cases where 2 line profiles were detected in the same spectrum, which are designated by "a" and "b" after the 2MASS source name, see Sect. 4.5. For marginal detections, the H I spectra are shown in Fig. 2.

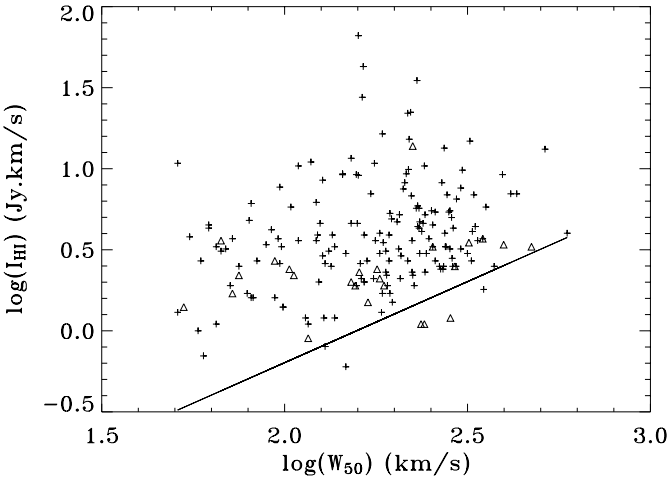

Fig. 3. Distribution of integrated H I line fluxes $I_{\rm HI}$ as a function of the H I line FWHM, W_{50}. The straight line indicates the 3 σ detection limit for a 250 km s^{-1} wide, flat-topped spectral line, based on the average rms noise level of the data. Clear detections of survey galaxies are represented by crosses, and marginal detections by triangles.

A description of all parameters listed in the tables is given below in Sects. 4.1–4.4. The near-infrared data listed were taken from the 2MASS catalogue and the optical data were taken from the online NED and LEDA databases, as indicated.

The distribution of the integrated line fluxes and FWHM's of the clear and marginal detections is shown in Fig. 3. Also plotted in this figure is a straight line indicating the 3σ detection limit for a 250 km s^{-1} wide, flat-topped spectral line, based on the average rms noise level of the data. The data quality and the rms noise in the observations is not very uniform in general, not even for the spectra in which detections were made, resulting in the dispersion among the weakest clear and marginal detections.

4.1. Names, positions and distances

• Number: we have divided the selected 2MASS sources according to two criteria: size and algorithm. This division is indicated by two characters in the galaxy designations which we will use throughout this series: "L" indicates that all objects we observed at Nançay are "Large" object with an isophotal $K_{\rm s}$-band radius $r_{K_{20}}$ (see Sect. 4.2) larger than 20″ (note that no "Small" sources, with a radius between 10″ and 20″, were observed at Nançay) and an "F" a galaxy selected using the LCSB source processor, while following the source number an "O" indicates a previously catalogued object, a "P" one with a PGC entry only and an "N" a previously uncatalogued one.
• Identifications: for each of the 2MASS sources we queried the NED and LEDA databases for a cross-identification of its position with other catalogues. For previously catalogued objects we list the most commonly used identification besides the 2MASS identification.
• Positions: the listed right ascensions and declinations are the catalogued 2MASS source centre positions, for epoch J2000.0.

These were used as the pointing centres for the H I observations.

• Distances: for each detected galaxy, a distance D was calculated using radial H I velocities corrected to the Galactic Standard of Rest, following the procedure given in the RC3 (and used in LEDA), and assuming a Hubble constant of H_0 = 75 km s^{-1} Mpc^{-1}.

4.2. Near-infrared data

• K_{20} is the total magnitude measured within the $r_{K_{20}}$ isophotal aperture (see below);

• $J-K$ is the $(J-K)_{20}$ near-infrared colour, based on magnitudes measured in the J and K_s bands within their respective isophotal semi-major axes at the 20 mag arcsec^{-2} level;

• μ_{K_s} is the mean central surface brightness (in mag arcsec^{-2}) measured within a radius of 5 arcsec around the source's centre;

• b/a is the infrared axis ratio determined from an ellipse fit to the co-addition of the J-, H-, and K_s-band images. The fit is carried out at the 3-σ isophotal level relative to the background noise in each image. The 2MASS F (LCSB sources) sample was not measured in this way because of the low signal-to-noise levels of the emission;

• $r_{K_{20}}$ is the fiducial aperture (in arcsec) in K band. Essentially, it is the aperture size for a surface brightness of 20 mag arcsec^{-2} in K band;

• L_K is the absolute magnitude in the K band (in $L_{\odot,K}$), calculated using an absolute solar K-band magnitude of 3.33 (Allen 1973).

4.3. Optical data

• Type is the morphological type, as listed in NED;

• $V_{\rm opt}$ is the mean heliocentric radial velocity (in km s^{-1}), as listed in LEDA;

• D_{25} is the isophotal B-band diameter (in units of arcmin) measured at a surface brightness level of 25 mag arcsec^{-2}, as listed in LEDA;

• B_{T_c} is the total apparent B-band magnitude reduced to the RC3 system (de Vaucouleurs et al. 1991) and corrected for galactic extinction, inclination and redshift effects (see Paturel et al. 1997, and references therein), as listed in LEDA;

• $\mu_{B_{25}}$ is the mean B-band surface brightness (in mag arcsec^{-2}) within the 25 mag arcsec^{-2} isophote, as listed in LEDA;

• L_B is the absolute magnitude in the B band (in $L_{\odot,B}$), calculated using the B_{T_c} magnitude and an absolute solar magnitude in the B band of 5.48 (Allen 1973), as listed in LEDA.

4.4. H I data

The global H I line parameters are directly measured values; no corrections have been applied to them for, e.g., instrumental resolution or cosmological stretching (e.g., Matthews et al. 2001)

• rms is the rms noise level in a spectrum (in mJy);

• $I_{\rm HI}$ is the integrated line flux (in Jy km s^{-1}). The upper limits listed are 3σ values for flat-topped profiles with a width of 250 km s^{-1}, a representative value for the galaxies detected;

• $V_{\rm HI}$ is the heliocentric central radial velocity of a line profile (in km s^{-1}), in the optical convention. We estimated the uncertainty, $\sigma_{V_{\rm HI}}$ (in km s^{-1}), in $V_{\rm HI}$ following Fouqué et al. (1990), as

$$\sigma_{V_{\rm HI}} = 4R^{0.5}P_W^{0.5}X^{-1} \quad (1)$$

where R is the instrumental resolution (~17 km s^{-1}, see Sect. 3.1), $P_W = (W_{20}–W_{50})/2$ (in km s^{-1}) and X is the signal-to-noise ratio of a spectrum, which we defined as the ratio of the peak flux density and the rms noise;

• V_0 is the H I radial velocity (in km s^{-1}) corrected to the Galactic Standard of Rest, following the RC3;

• W_{50} and W_{20} are the velocity widths (in km s^{-1}) at 50% and 20% of peak maximum (km s^{-1}). According to Fouqué et al. (1990), the uncertainty in the line widths is $2\sigma_{V_{\rm HI}}$ (see above) for W_{50} and $3\sigma_{V_{\rm HI}}$ for W_{20}.

• $M_{\rm HI}$ is the total H I mass (in $M_\odot$), $M_{\rm HI} = 2.356 \times 10^5 D^2\ I_{\rm HI}$;

• $M_{\rm HI}/L_B$ is the ratio of the total H I mass to the B-band luminosity (in $M_\odot/L_{\odot,B}$);

• $M_{\rm HI}/L_K$ is the ratio of the total H I mass to the K_s-band luminosity (in $M_\odot/L_{\odot,K}$).

4.5. Notes on individual galaxies

In order to identify possible confused sources in our H I observations, we first inspected DSS images over a region of $12' \times 36'$ ($\alpha \times \delta$) centred on the 2MASS position of each clearly or marginally detected source. In case galaxies were noted that might give rise to confusion with the H I profile of the target galaxy, we queried the NED and LEDA databases for data on the objects. The data listed here were preferentially taken from the mean values listed in LEDA. The global H I line parameters of galaxies reported as detected in the literature are listed in Table 2.

L6O: 2MASX J00140398–2310555 = NGC 45: the 2MASS source is a bright H II region in the outer disc of this large (D_{25} = 7.′4) spiral, whose E-W extent far exceeds the 3.′6 Nançay HPBW. This explains why our integrated H I line flux of 66 Jy km s^{-1}, is much lower than the mean literature value of 245 Jy km s^{-1} (LEDA), which was measured with larger telescope beams covering the entire galaxy.

L29O: 2MASXI J0041576–325810 = ESO 351–G2: our H I detection ($V_{\rm HI}$ = 9560 km s^{-1}, W_{50} = 193: km s^{-1}) appears to have its high-velocity edge reduced by negative RFI, and it may be confused by a nearby galaxy. The target galaxy ($V_{\rm opt}$ = 9618 ± 49 km s^{-1}, B_T = 15.27, D_{25} = 0.′9), has an edge-on companion at 1.′1 separation, MCG-6-2-24 ($V_{\rm opt}$ = 9525 ± 60 km s^{-1}, B_T = 16.55, D_{25} = 0.′6); both are classified as Sc spirals. Both galaxies have a systemic velocity corresponding to the H I velocity, within the errors, but the companion is 1.3 mag weaker.

L57O: 2MASX J01190447–0008190 = UGC 847: our H I detection ($V_{\rm HI}$ = 5238 km s^{-1}, W_{50} = 271 km s^{-1}) may be slightly confused by a nearby galaxy. The edge-on target

galaxy, (V_{opt} = 5218 ± 60 km s^{-1}, B_T = 16.29, D_{25} = 1′.4, Scd) has a companion 3′.5 East of it, i.e. well outside the telescope's HPBW, PGC 212709 (V_{opt} = 5173 ± 22 km s^{-1} [Sloane Survey], B_T = 16.27, D_{25} = 0′.6).

L59O: 2MASX J01222287–3636297 = ESO 352-G58: our H I profile may in principle be confused, as at only 0′.5 from the centre of the target galaxy, (B_T = 15.82, D_{25} = 1′.2, Sbc), lies the much smaller Irr galaxy PGC 634708 (B_T = 17.75, D_{25} = 0′.35). Neither has a known optical redshift, however.

L70O: 2MASX J01430297–3411143 = IC 1722: though our H I profile looks rather complex, with V_{HI} = 3911 km s^{-1} and W_{50} = 515 km s^{-1}, it does not seem likely it is confused with two nearby early-type galaxies. The target galaxy (V_{opt} = 4082 ± 35 km s^{-1}, B_T = 14.68, D_{25} = 1′.5, SBbc), is highly inclined, as are nearby IC 1724 (V_{opt} = 3836 ± 51 km s^{-1}, B_T = 14.53, D_{25} = 1′.2, S0), 3′.6 to the south, and ESO 353–G36 (V_{opt} = 3774 ± 137 km s^{-1}, B_T = 15.11, D_{25} = 1′.0, SO-a), 3′.4 to the east, outside the HPBW. Although the systemic velocities of the latter two objects are closer to the H I velocity, they are both classified as lenticulars and therefore not expected to be gas-rich.

L86O: 2MASX J01590735–0308587 = MCG -1-6-13: 1′.1 east of the target galaxy MCG -1-6-13 (V_{opt} = 5342 ± 42 km s^{-1}, B_T = 14.71, D_{25} = 1′.0, Irr), lies an Sa spiral of unknown velocity, KUG 0156-033 (B_T = 15.22, D_{25} = 0′.55, Sa).

L117O: 2MASX J02284546-1030501 = NGC 948: our H I profile of this object (V_{HI} = 4758 km s^{-1}, W_{50} = 168 km s^{-1}, I_{HI} = 5.0 Jy km s^{-1}) is probably confused with that of its larger neighbour NGC 945. At 2′.5 from the target galaxy (V_{opt} = 4511 ± 43 km s^{-1}, B_T = 14.38, D_{25} = 1′.2, SBc), lies the larger spiral NGC 945 (V_{opt} = 4484 ± 60 km s^{-1}, B_T = 12.89, D_{25} = 2′.2, SBc). At Nançay Theureau et al. (1998) detected NGC 945 (V_{HI} = 4482 km s^{-1}, W_{50} = 179 km s^{-1}, I_{HI} = 4.0 Jy km s^{-1}), while at Arecibo Haynes et al. (1999) detected NGC 948 (W_{50} = 181 km s^{-1}, I_{HI} = 6.0 Jy km s^{-1}). The E-W HPBW of the two telescopes is quite similar, 3′.6, and serious confusion is inevitable between the line signal of both galaxies, whose centres are separated by 2′.5.

(L125O): 2MASXi J0235204+405522 = NGC 980: this object is classified as an S0 and therefore unlikely to be detectable in H I, and our H I spectrum (V_{HI} = 5744 km s^{-1}, W_{50} = 592 km s^{-1}, I_{HI} = 4.0 Jy km s^{-1}) is confused by nearby galaxies. Within the same telescope beam as the target object (V_{opt} = 5796 ± 42 km s^{-1}, B_T = 14.27, D_{25} = 1′.7), lies the Sa spiral NGC 982 (V_{opt} = 5845 ± 52 km s^{-1}, B_T = 13.16, D_{25} = 1′.5) at 3′.3, the Sd spiral UGC 2068 (B_T = 17.68, D_{25} = 0′.75) at 2′.1 and the SBb spiral MCG +7-6-40 (B_T = 17.96, D_{25} = 0′.35) at 4′.2 distance; the latter two do not have a known redshift. NGC 980 was detected at Arecibo (V_{HI} = 5757 km s^{-1}, W_{50} = 702 km s^{-1}, I_{HI} = 8.2 Jy km s^{-1}; Haynes et al. 1988), NGC 982 also at Arecibo (V_{HI} = 5737 km s^{-1}, W_{50} = 568 km s^{-1}, I_{HI} = 7.0 Jy km s^{-1}; Magri 1994) and UGC 2068 at Nançay (V_{HI} = 5740 km s^{-1}; Theureau et al. 1998). Seen the similar optical redshifts of NGC 980 and 982 and their proximity all published H I profiles of these objects must be confused.

L161O: 2MASXI J0306290–094332 = IC 1880: it is not clear to which galaxy our H I detection (V_{HI} = 3935 km s^{-1}, W_{50} = 144 km s^{-1}, I_{HI} = 9.2 Jy km s^{-1}) is due. The target galaxy is a lenticular at V_{opt} = 10 224 ± 42 km s^{-1}. There is one other galaxy in the beam, of unknown redshift, PGC 135017 (B_T = 16, D_{25} = 0′.7, Sc) and another outside the HPBW, NGC 1208 (V_{opt} = 4518 ± 53 km s^{-1}, B_T = 13.31, D_{25} = 1′.9), which has a too high redshift and is classified as SO/a. Only a weak H I line was detected towards NGC 1208 at Nançay by Theureau et al. (1998) : V_{HI} = 4356 km s^{-1}, W_{50} = 259 km s^{-1}, I_{HI} = 0′.5 Jy km s^{-1}.

L184O: 2MASX J03234832+4033485 = UGC 2708: it is not clear if the marginal H I detection (V_{HI} = 8582: km s^{-1}, W_{50} = 295: km s^{-1}, I_{HI} = 6.5: Jy km s^{-1}) is (mainly) due to residual RFI from the GPS L3 band centered on 8250 km s^{-1} (see Sect. 3.2.1), or to a galaxy. It is ∼3200 km s^{-1} higher than the optical redshift of the target galaxy, 5390 ± 51 km s^{-1}. Furthermore the galaxy has been classified as SB0 and is therefore unlikely to be detectable. There are no likely candidates for confusion in the vicinity. We therefore consider this a tentative detection only.

L203O: 2MASX J03404154–2239041 = ESO 482–G31: our narrow H I detection (V_{HI} = 1683 km s^{-1}, W_{50} = 60 km s^{-1}, I_{HI} = 0.5 Jy km s^{-1}) may be due to a nearby galaxy. The target galaxy (V_{opt}1629 ± 43 km s^{-1}, B_T = 15.27, D_{25} = 0′.9) is classified as an S0. At the edge of the beam lies the much larger NGC 1415 (V_{opt} = 1549 ± 47 km s^{-1}, B_T = 12.77, D_{25} = 3′.3). Though classified as S0/a, it has quite a strong H I line as detected, respectively, at Nançay (Balkowski 1979) and Effelsberg (Huchtmeier 1982): mean values V_{HI} = 1585 km s^{-1}, W_{50} = 322 km s^{-1} and I_{HI} = 8.3 Jy km s^{-1}.

L237O: 2MASX J04294085–2724313 = NGC 1592: this Irregular object appears to be a merger or a very close, interacting pair of galaxies.

L249O: 2MASXI J0443334–274006 = ESO 421–G13: our H I spectrum shows two peaks, at V_{HI} = 5353 and 10 457 km s^{-1}, respectively. The target galaxy (B_T = 15.3, D_{25} = 1′.2, Sbc) does not have a known optical redshift; there is no other candidate for confusion within the beam in the search area. Seen its size and magnitude, an association with the 5353 km s^{-1} profile seems the most likely.

L255O: 2MASX J04511837–0557379 = MCG -01-13-021: one nearby galaxy, 2MASXi J0451123–060013, lies within the beam, while two others lie on the edge of the beam: MCG -01-13-020 (B_T = 15.29, D_{25} = 1′.0) and 2MASXi J0451085–060321. Like the target galaxy (B_T = 15.23, D_{25} = 1′.5, Sc), none of these have a known redshift.

L256O: 2MASX J04551547–1209275 = MCG -2-13-23: it is not clear to which of the two galaxies in the telescope beam galaxy our detection (V_{HI} = 4862 km s^{-1}, W_{50} = 231 km s^{-1}, I_{HI} = 4.4 Jy km s^{-1}) is due, as the target galaxy has an optical redshift of 17 881 ± 60 km s^{-1} (Huchra et al. 1993), which is far outside our velocity search range, while the other galaxy in the beam, MCG -2-13-22, is an S0 with V_{opt} = 8133 ± 60 km s^{-1}. The observed line signal may be spurious and due imperfectly filtered out RFI.

L272O: 2MASX J05153881–2242320 = ESO 486–G40: it seems unlikely that our detection is confused by the one magnitude weaker AM 0513-224, of unknown redshift, at the edge

of the beam. Our H I redshift of the target galaxy, 5796 km s^{-1}, corresponds to its optical value of 5779 ± 42 km s^{-1}.

L297O: 2MASX J06131885+5306445 = UGC 3421: it is not clear if our H I detection of the target galaxy (D_{25} = 0.′9, Sd) may be confused by a galaxy at the edge of the beam (at 3.′3 EW separation), UGC 3424 (B_T = 16.24, D_{25} = 1.′2, Irr), as neither has a published redshift.

L302O: 2MASX J06243891–2235497 = ESO 489-G50: The target galaxy (V_{opt} = 2892 km s^{-1}, B_T = 15.79, D_{25} = 1.′4), is classified as S0-a and therefore unlikely to be gas-rich. Our H I detection (V_{HI} = 2713 km s^{-1}, W_{50} = 316 km s^{-1}, I_{HI} = 9.8 Jy km s^{-1}) appears due to a large galaxy at the edge of the beam, 14.′4 south of the target galaxy, NGC 2223 (V_{opt} = 2690 ± 61 km s^{-1}, B_T = 12.51, D_{25} = 2.′9, SBc), whose mean H I profile parameters are V_{HI} = 2721 km s^{-1}, W_{50} = 300 km s^{-1} and I_{HI} = 26 Jy km s^{-1} (Bottinelli et al. 1982; Fisher & Tully 1981; Staveley-Smith & Davies 1987).

L336O: 2MASXI J0819021+211122 = UGC 4329: the redshift of our H I detection (V_{HI} = 4079 km s^{-1}, W_{50} = 222 km s^{-1}, I_{HI} = 6.8 Jy km s^{-1}) is in agreement with the V_{opt} = 4144 ± 73 km s^{-1}, and the spectrum is unlikely to be confused by the 4 galaxies that lie at the edge of the beam (CGCG 119-043, CGCG 119-053, NGC 2556 and NGC 2557) as they all have redshifts in the range of 4460–4860 km s^{-1}. Its line parameters agree with the published mean values of V_{HI} = 4097 km s^{-1}, W_{50} = 223 km s^{-1} and I_{HI} = 8.7 Jy km s^{-1} (Bicay & Giovanelli 1986; Bothun et al. 1985; Lewis 1983; Lewis et al. 1985; Rosenberg & Schneider 2000; Schommer et al. 1981; Tifft & Cocke 1988).

L345O: 2MASX J08325749–2254031 = ESO 495–G17: our H I detection (V_{HI} = 1416 km s^{-1}, W_{50} = 205 km s^{-1}, I_{HI} = 3.2 Jy km s^{-1}) may be due to gas in the outer disc of the nearby large spiral NGC 2613. Another Nançay spectrum (Chamaraux et al. 1999) of our target galaxy (B_T = 14.76, D_{25} = 1.′4, Sb), of unknown redshift, shows W_{50} = 178 km s^{-1} and I_{HI} = 3.9 Jy km s^{-1}. Although the centre of NGC 2613 (V_{opt} = 1599 ± 88 km s^{-1}, B_T = 11.15, D_{25} = 7.′0) lies 7.′3 SE of that of the target galaxy, its diameter is large enough to cause confusion. H I observations of NGC 2613 (Bottinelli et al. 1982; Fisher & Tully 1981; Reif et al. 1982; Staveley-Smith & Davies 1987) show mean parameters of V_{HI} = 1678 km s^{-1}, W_{50} = 599 km s^{-1} and I_{HI} = 83 Jy km s^{-1}.

L358O: 2MASX J08565629–2031383 = ESO 563–G34: our narrow H I profile (V_{HI} = 2616 km s^{-1}, W_{50} = 97 km s^{-1}, I_{HI} = 4.4 Jy km s^{-1}) of the target galaxy (V_{opt} = 2558 ± 60 km s^{-1}, B_T = 14.32, D_{25} = 1.′2, Sab) does not appear to be confused by a galaxy on the edge of the beam, at ∼3′ E-W separation, ESO 563-G36 (V_{opt} = 2656 ± 50 km s^{-1}, B_T = 13.88, D_{25} = 1.′4, Sab).

L360O: 2MASX J09001445+3543527 = NGC 2719: confused H I spectrum. The target galaxy (V_{opt} = 3172 ± 46 km s^{-1}, B_T = 13.65, D_{25} = 1.′2, Irr), forms a close pair (0.′5 separation) with NGC 2719A (V_{opt} = 3069 ± 43 km s^{-1}, B_T = 14.50, D_{25} = 0.′55, Irr). Surprisingly, our H I detection (V_{HI} = 3043 km s^{-1}, W_{50} = 215 km s^{-1}, I_{HI} = 9.3 Jy km s^{-1}) has a 114 km s^{-1} lower central velocity and a two times smaller integrated line flux than the Arecio profile of Bicay & Giovanelli (1986), with V_{HI} = 3157 km s^{-1}, W_{50} = 231 km s^{-1} and I_{HI} = 17.9 Jy km s^{-1}, which also includes both galaxies.

L371O: 2MASXI J0917317+415932 = NGC 2799: our H I profile is confused, as there are two other sizeable galaxies of similar redshift in the beam of the target galaxy (V_{opt} = 1860 ± 68 km s^{-1}, B_T = 13.98, D_{25} = 1.′8, SBd): NGC 2798 (V_{opt} = 1735 ± 67 km s^{-1}, B_T = 14.92, D_{25} = 2.′7, SBa) and UGC 4904 (V_{opt} = 1644 ± 60 km s^{-1}, B_T = 15.21, D_{25} = 1.′0, SBbc). The E-W separation between NGC 2799/98 is 1.′6, i.e. only about half the Nançay HPBW. Our H I profile has V_{HI} = 1616 km s^{-1}, W_{50} = 159 km s^{-1} and I_{HI} = 9.1 Jy km s^{-1}, while the Nançay profile of NGC 2799 from Bottinelli et al. (1982) has V_{HI} = 1755 km s^{-1}, W_{50} = 340 km s^{-1} and I_{HI} = 11.1 Jy km s^{-1} and a Nançay profile of NGC 2798 (Bottinelli et al. 1980) has V_{HI} = 1726 km s^{-1}, W_{50} = 313 km s^{-1} and I_{HI} = 11.5 Jy km s^{-1}. Our profile has a ∼125 km s^{-1} lower central velocity and a two times smaller W_{50}. Profiles that include the three above-mentioned galaxies were published by Huchtmeier (1982) and Peterson & Shostak (1974).

(F26O) = MCG -1-25-33: our H I profile is probably confused, since there is a pair of galaxies, of unknown redshift, of similar size in the beam of the target galaxy (B_T = 14.48, D_{25} = 1.′3, SBcd): UGC A 173 (V_{opt} = 1875 ± 97 km s^{-1}, B_T = 14.63, D_{25} = 1.′3, SBd) and UGC A 174 (B_T = 14.85, D_{25} = 1.′3, SBm). Our H I profile (V_{HI} = 1883 km s^{-1}, W_{50} = 118 km s^{-1}, I_{HI} = 11.0 Jy km s^{-1}) agrees with the Richter & Huchtmeier (1987) Effelsberg profile of UGC A 173 (V_{HI} = 1867 km s^{-1}, W_{50} = 189 km s^{-1}, I_{HI} = 12.7 Jy km s^{-1}), which includes all three objects.

L392O: 2MASX J09450315–0429475 = FGC 936: there are two galaxies, both of unknown redshift, with only 0.′6 separation at the centre of the beam, FGC 936 (B_T = 16.6, D_{25} = 0.′9, Sc) and 2MASXi J0945014–042919 (=PGC 1057506), with B_T = 16.45 and D_{25} = 0.′5). While in NED the position of our 2MASS source coincides exactly with that of FGC 936, in LEDA it coincides exactly with that of the other galaxy. As the LEDA positions all have an accuracy of 10″, significantly better than that from the FGC (Karachentsev et al. 1999), we adopted the latter association.

L403O: 2MASX J10144367–2048367 = ESO 567–G28: our H I profile (V_{HI} = 3705 km s^{-1}, W_{50} = 208 km s^{-1}, I_{HI} = 2.9 Jy km s^{-1}) may in principle be confused. At about the HPBW level of our beam, pointed at the target galaxy (B_T = 15.43, D_{25} = 1.′2, Sbc) lie two galaxies, also of unknown redshift: ESO 567-G28 (B_T = 15.87, D_{25} = 0.′6, Sbc) and 2MASXi J1014531-205752 (=PGC 834527), with B_T = 16.19 and D_{25} = 0.′8.

L447O: 2MASX J11174025+3803095 = UGC 6307: our profile has a 58 km s^{-1} lower central velocity than the Green Bank 91m profile of Schneider et al. (1992), although the W_{50} line widths are the same (206 km s^{-1}). The Nançay integrated line flux is 1.4 times higher. No candidates for confusion within the telescope beams are visible on the DSS.

L455O: 2MASXI J1128100+165531 = NGC 3691: our profile (V_{HI} = 987 km s^{-1}) has an on average 100 km s^{-1} lower central velocity than the 4 published H I spectra, three of which were measured at Arecibo and one with the Green Bank 91m telescope (see Table 2). The line widths and integrated line

fluxes are in agreement, however. The optical systemic velocity of 997 ± 38 km s^{-1} (Blackman 1980) is in good agreement with our centre velocity. The Nançay profile has a peculiar shape and may in principle have been affected by RFI. No candidates for confusion within the telescope beams are visible on the DSS.

L459O: 2MASX J11375027+4752539 = NGC 3769A: the H I profile of the target galaxy is confused with that of NGC 3769, the much larger spiral with which it forms a close pair. Our H I profile (V_{HI} = 734 km s^{-1}, W_{50} = 230 km s^{-1}, I_{HI} = 35.0 Jy km s^{-1}) is in agreement with the mean of the literature values of V_{HI} = 732 km s^{-1}, W_{50} = 232 km s^{-1} and I_{HI} = 50.6 Jy km s^{-1} (Magri 1994; Rhee & van Albada 1996; Verheijen & Sancisi 2001). The latter refers to a mapping of the pair with the WSRT.

L481O: 2MASX J11562491–1210003 = MCG -02-31-002: our H I spectrum shows two peaks, at V_{HI} = 5429 and 11 891 km s^{-1}, respectively. The latter detection appears to have its high-velocity edge clipped by negaative RFI. The target galaxy (B_T = 15.4, D_{25} = 1.′2) does not have a known optical redshift and there is no other galaxy in the search area likely to cause confusion in the Nançay beam.

L497O: 2MASXI J1212205+291240 = NGC 4173: our H I spectrum shows two detections, at V_{HI} = 1054 and 3795 km s^{-1}, respectively. The former is due to the target galaxy, at V_{opt} = 1117 ± 32 km s^{-1}, while the latter is due to three other galaxies in the beam (NGC 4169, 4174 and 4175), which have optical redhifts in the range of 3780–4000 km s^{-1}. The redshift of our profile of NGC 4173 (V_{HI} = 1054 km s^{-1}, W_{50} = 163 km s^{-1}, I_{HI} = 27.6 Jy km s^{-1}) is 53 km s^{-1} higher than the mean LEDA values (V_{HI} = 1107 km s^{-1}, W_{50} = 116 km s^{-1}, I_{HI} = 13.4 Jy km s^{-1}) and its integrated line flux is twice as high.

L502P: 2MASXI J1216418–251505 = PGC 781011: two peaks are seen in our H I spectrum, at 451 and 5708 km s^{-1}, respectively. On the DSS no obvious candidate could be found that might correspond to the former H I signal (V_{HI} = 451 km s^{-1}, W_{50} = 65 km s^{-1}, I_{HI} = 1.1 Jy km s^{-1}). We assume that the latter peak (V_{HI} = 5708 km s^{-1}, W_{50} = 62 km s^{-1}, I_{HI} = 1.6 Jy km s^{-1}) corresponds to the target galaxy (B_T = 16.1, D_{25} = 0.′5).

L548O: 2MASX J12503459–0931108 = MCG -01-33-022: our H I profile of the target galaxy (V_{HI} = 4689 km s^{-1}, W_{50} = 274 km s^{-1}, I_{HI} = 4.0 Jy km s^{-1}), with an optical redshift of 4666 ± 80 km s^{-1}, is very probably confused with that of a nearby pair of galaxies, NGC 4716/7. NGC 4716 is an S0 with V_{opt} = 4573 ± 119 km s^{-1} and NGC 4717 is a spiral with V_{opt} = 4515 ± 96 kms; none of them has previously been reported as detected in HI.

L569O: 2MASX J13165624–1635347 = MCG -03-34-040: the target galaxy is seen superposed on the outermost regions of a much larger Sbc spiral, NGC 5054, which will dominate the H I profile. Our H I line parameters (V_{HI} = 1682 km s^{-1}, W_{50} = 321 km s^{-1}, I_{HI} = 14.8 Jy km s^{-1}) are quite different the mean published values of NGC 5054 V_{HI} = 1741 km s^{-1}, W_{50} = 315 km s^{-1}, I_{HI} = 26.8 Jy km s^{-1} (Bottinelli et al. 1982; Fisher & Tully 1981; Richter & Huchtmeier 1987; Shostak 1978).

L582O: 2MASX J13324730+4151564 = ESO 579–G5: the target galaxy is seen superposed on the outer regions of a much larger Sc spiral, NGC 5214, which will dominate the H I profile. Our H I line parameters (V_{HI} = 8174 km s^{-1}, W_{50} = 303 km s^{-1}, I_{HI} = 7.6 Jy km s^{-1}) are similar to the published values of NGC 5124 V_{HI} = 8180 km s^{-1}, W_{50} = 306 km s^{-1}, I_{HI} = 4.9 Jy km s^{-1} (Haynes & Giovanelli 1991). In the same beam as the target galaxy (B_T = 15.8, D_{25} = 1.′0, Sbc), lies the somewhat fainter Sab ESO 579-G6 (B_T = 16.2, D_{25} = 0.′8). Since neither has a known optical redshift, it cannot be determined if their proximity could cause confusion in our H I spectrum.

(F40O) = MCG -2-36-13: the radial velocity of the detected line profile, 4882 km s^{-1}, is completely different from the optical value of 12 500 km s^{-1} (da Costa et al. 1998), which lies far outside our velocity search range. No candidate was found for confusion within the beam. The observed line signal may be spurious and due imperfectly filtered to RFI.

L643O: 2MASXI J1447561–141658 = MCG -02-38-015: the target object corresponds to an outer spiral arm of the spiral MCG -02-38-015. Our H I profile parameters (V_{HI} = 1927 km s^{-1}, W_{50} = 221 km s^{-1}, I_{HI} = 22.3 Jy km s^{-1}) show a 66 km s^{-1} lower mean velocity than the average of the literature values, V_{HI} = 2046 km s^{-1}, W_{50} = 199 km s^{-1} and I_{HI} = 23.4 Jy km s^{-1} (Theureau et al. 1998; Thonnard et al. 1978).

L647O: 2MASX J14563333–2430079 = ESO 513–G009: our H I spectrum shows two peaks, at V_{HI} = 6894 and 8600 km s^{-1}, respectively. The optical redshift of the target galaxy, 6815 ± 44 km s^{-1}, corresponds to the lower velocity peak. No galaxy could be identified that may have caused the other peak.

L651O: 2MASX J15064639+1251009 = CGCG 077-007: the H I profile of the target galaxy, (V_{opt} = 6582 ± 105 km s^{-1}, B_T = 16.1, D_{25} = 0.′7) will be confused with that of NGC 5851 (V_{opt} = 6515 ± 64 km s^{-1}, B_T = 14.2, D_{25} = 1.′0), at 1.′8 E of the 2MASS object, i.e. around the Nançay HPBW. Our H I profile shows V_{HI} = 6576 km s^{-1}, W_{50} = 43 km s^{-1} and I_{HI} = 5.5 Jy km s^{-1}, while the Nançay profile of NGC 5851 (Bottinelli et al. 1999) shows V_{HI} = 6508 km s^{-1}, W_{50} = 281 km s^{-1} and I_{HI} = 2.3 Jy km s^{-1}.

L654P: 2MASX J15205260–2859139 = PGC 160462: our H I spectrum shows two peaks, at V_{HI} = 3934 and 6022 km s^{-1}, respectively. The target galaxy has no known optical redshift and no other galaxy was found in the search area. It is not clear with which of the two H I lines it is associated.

L705O: 2MASXI J1719223+490202 = VV 010b: our H I spectrum (V_{HI} = 7478 km s^{-1}, W_{50} = 97 km s^{-1}, I_{HI} = 2.6 Jy km s^{-1}) will be confused by that of the interacting pair Arp 102 (PGC 60067/70); the centre of PGC 60070 lies only 0.′5 from that of the much smaller Sd target galaxy, PGC 60073 (B_T = 16.2, D_{25} = 0.′7) PGC 60070 is an Sd with V_{opt} = 7177 ± 35 km s^{-1}, B_T = 15.5 and D_{25} = 1.′1, and PGC 60067 an elliptical with V_{opt} = 7304 ± 99 km s^{-1}, B_T = 15.5 and D_{25} = 0.′95.

L712O: 2MASX J18030213+2922257 = CGCG 171-049: the H I spectrum (V_{HI} = 7048 km s^{-1}, W_{50} = 473 km s^{-1}, I_{HI} = 3.3 Jy km s^{-1}) of the target galaxy (V_{opt} = 7048 ±

46 km s^{-1}, B_T = 15.7, D_{25} = 0.′8) may be confused by another galaxy in the telescope beam, CGCG 171-048 (V_{opt} = 6983 ± 44 km s^{-1}, B_T = 15.4, D_{25} = 0.′75).

L745O: 2MASX J20170275–1206516 = MCG -02-51-007: the H I spectrum (V_{HI} = 5656 km s^{-1}, W_{50} = 355 km s^{-1}, I_{HI} = 5.8 Jy km s^{-1}) of the target galaxy (B_T = 15.6, log(D_{25} = 0.′8, Sb), without known optical redshift, may be confused by another galaxy in the telescope beam, MCG -02-51-008 (V_{opt} = 5578 ± 60 km s^{-1}, B_T = 14.3, D_{25} = 0.′6, Sc).

L752O: = FGC 2286: our profile has a 43 km s^{-1} lower central velocity than the Nançay profile of Matthews & van Driel (2000), although the line widths and integrated line fluxes are comparable (see Table 2).

L755O: 2MASX J20481195–0352186 = MCG -01-53-009: the H I spectrum (V_{HI} = 6042 km s^{-1}, W_{50} = 128 km s^{-1}, I_{HI} = 1.2 Jy km s^{-1}) of the target galaxy (V_{opt} = 5945 ± 60 km s^{-1}, B = 13, D_{25} = 1.′1), may in principle be confused by an object of similar size but lower surface brightness at only 0.′9 separation, MCG -01-53-010 (B = 15, D_{25} = 1.′0), without known redshift.

L758O: 2MASX J20550682–3105304 = ESO 463–IG34: the target galaxy is a close interacting pair of galaxies.

L766O: 2MASX J21455799–3448541 = ESO 403–G23: our H I spectrum shows two peaks, at V_{HI} = 5140 and 12 924 km s^{-1}, respectively. No other galaxy was found in the search area besides the target galaxy (B_T = 15.4, D_{25} = 1.′2, Sc), without known optical redshift. Seen the galaxy's optical parameters, it is most likely with the H I emission at 5140 km s^{-1}.

L777P: 2MASXI J2216009–095612 = PGC 984498: the target galaxy (B_T = 16.5, D_{25} = 0.′5), shows two nuclei on the DSS and 2MASS images, as well as a tidal tail on the DSS. There is another galaxy of similar magnitude in the beam, 2MASXi J2216005-095324 (B_T = 16.5, D_{25} = 0.′9), also without optical redshift.

L783O: 2MASX J22230550–2857173 = NGC 7259: the H I spectrum (V_{HI} = 1657 km s^{-1}, W_{50} = 152 km s^{-1}, I_{HI} = 11.6 Jy km s^{-1}) of the target galaxy (V_{opt} = 1718 ± 42 km s^{-1}, B_T = 13.6, D_{25} = 1.′2), will be confused by an edge-on galaxy at 2.′8 distance, ESO 467-G51 (V_{opt} = 1775 ± 32 km s^{-1}, B_T = 14.6, D_{25} = 2.′8), of which Theureau et al. (1998) obtained an H I profile at Nançay with V_{HI} = 1808 km s^{-1}, W_{50} = 146 km s^{-1}, I_{HI} = 18.6 Jy km s^{-1}.

L794O: 2MASXI J2244347–225930 = ESO 534–G21: the H I profile of the target galaxy will not be confused by its close apparent companion, ESO-LV 5340211 at only 0.′3 distance, as their optical redshifts are 3159 and 18 116 km s^{-1}, respectively.

5. Discussion

A comparison of the global parameters of the H I profiles measured for our survey at Nançay with those obtained from the literature is given in Table 2. Indicated with a "*" after the source name in Col. 1 are the cases in which profile(s) are likely to be confused with those of other galaxies in the telescope beam(s), see Sect. 4.5 for further details. We also compared the line parameters of the 18 calibrator galaxies observed throughout the survey.

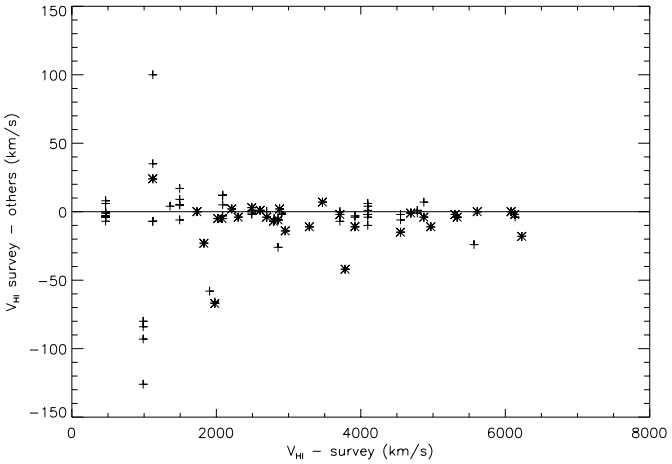

Fig. 4. Comparison of central H I profile velocities, V_{HI}, of survey and calibration galaxies with literature values (see Table 2). Plotted is the difference (survey-others) as function of the H I radial velocity measured in the survey. To guide the eye, a horizontal line was plotted at ΔV = 0 km s^{-1}; this line does not represent a fit to the data. Comparisons with published Nançay data are represented by a ⋆, the crosses indicate comparisons to measurements made with other telescopes.

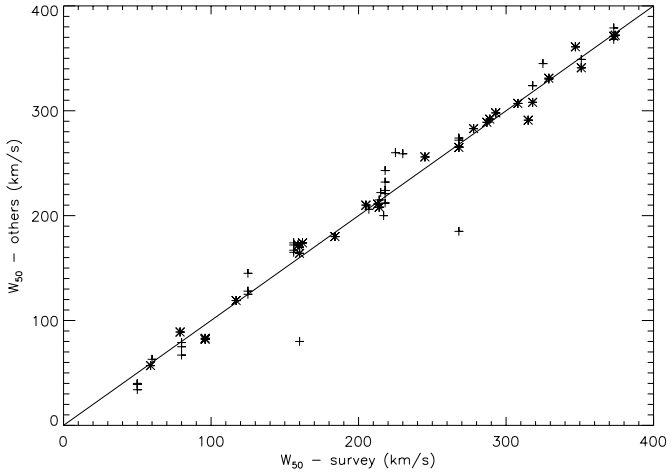

Fig. 5. Comparison of H I profile FWHMs, W_{50}, of survey and calibration galaxies with literature values (see Table 2). To guide the eye, a diagonal line with a slope of 1 was plotted; this line does not represent a fit to the data. Comparisons with published Nançay data are represented by a ⋆, the crosses indicate comparisons to measurements made with other telescopes.

Plotted in Figs. 4–6 are, respectively, the differences between central line velocities from our survey and from the literature, survey and literature W_{50} line widths and I_{HI} integrated line fluxes for the 2MASS survey galaxies with non-confused spectra as well as for the calibration galaxies.

The agreement between the central H I velocities is generally good (Fig. 4). The 4 survey galaxies for which the literature values are (on average) more than 40 km s^{-1} different from our values are L447O (UGC 6307), L455O (NGC 3691), L643O (MCG 2-38-15) and L752O (FGC 2286), see Sect. 4.5

Table 1. H I detection statistics.

	Previously catalogued (other)		Previously catalogued (PGC)		Previously uncatalogued (new)		All
	Large	Faint	Large	Faint	Large	Faint	
Total observed	229	14	41	0	39	11	334
Detected	140 61%	10 71%	12 29%	0 0%	5 13%	4 36%	171 51%
Marginal	23 10%	0 0%	0 0%	0 0%	0 0%	0 0%	24 7%
Undetected	66 29%	4 29%	29 71%	0 0%	34 87%	7 64%	139 42%

Note: large: galaxies with $r_{K_{20}} \geq 20''$, faint: galaxies selected using the LCSB source processor.

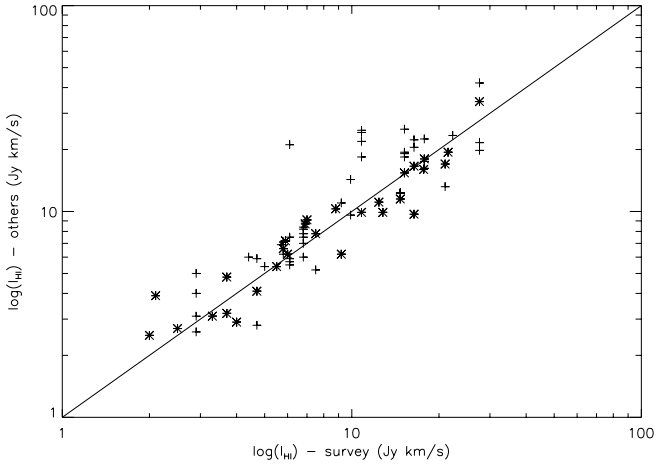

Fig. 6. Comparison of integrated H I line fluxes, $I_{\rm HI}$, of survey and calibration galaxies with literature values (see Table 2). To guide the eye, a diagonal line with a slope of 1 was plotted; this line does not represent a fit to the data. Comparisons with published Nançay data are represented by a $\star$, the crosses indicate comparisons to measurements made with other telescopes.

for comments. In general no clear cause can be identified for these discrepancies, although RFI in our data may be involved in some cases.

The agreement between the W_{50} line widths is generally good (Fig. 5), with two exceptions. These two discrepancies, of about -80 km s^{-1}, for L497O (NGC 4173) and calibration galaxy NGC 3321 (PGC 31653) are due to one anomalously narrow published line width per galaxy, while all other literature values are in agreement with ours.

A comparison between the integrated line fluxes $I_{\rm HI}$ (Fig. 6) shows a larger scatter for the survey objects than the two other plots, which appears reasonable, however, seen the dispersion found in other such plots (e.g., van Driel et al. 2000). The three cases in which a literature value exceed our measurement by more than a factor 2 are L6O (NGC 45), which is considerably larger than the Nançay beam, L445O (IC 2627), which may well have been resolved by the Nançay beam and L487O (UGC 7000), due to the anomalously high Arecibo value of Impey et al. (1996).

The fluxes of the calibrator galaxies are in good agreement with the literature values. Comparing to measurements made with other telescopes, which are available for 7 galaxies, we find that our $I_{\rm HI}$ values are on average 0.95 ± 0.25 times these values. Comparing to the Nançay measurements of 18 galaxies by Theureau et al. (1998), which were made with the previous receiver system (see Sect. 3), we find a scaling factor of 1.10 ± 0.22. The standard deviations in these scaling factors are only slightly larger than the $\sim\pm$15% accuracy of the internal calibration of the Nançay data (e.g., Matthews et al. 2001).

There are 4 survey galaxies (L180O = FGC 410, L467O = UGC 6679, L630O = ESO 447-5 and L673O = MCG 3-41-136) that did not meet our criteria for clear or marginal detections, which were reported as detected in the literature (see Table 2). All four were observed by us in the low-velocity search mode only, i.e. in the -500 to 10 500 km s^{-1} range, which means that the systemic velocity of L630O (10 600 km s^{-1}) lies just outside our search range. The other three were detected in the Nançay survey of Matthews & van Driel (2000), which has a significantly lower noise level than the present survey.

6. Conclusions

Of the 334 galaxies observed in total, 171 (51%) were clearly detected, 76 of which did not have a previously known radial velocity. The detection statistics as function of type (previously catalogued (PGC/other catalogues) or not) and size/selection algorithm (Large/Faint) are listed in Table 1. For the Large objects ($r_{K_{20}} \geq 20''$) and the Faint objects (selected with the LCSB source processor), the overall detection rates are quite similar: 51% and 56%, respectively.

Acknowledgements. This publication makes use of data products from the Two Micron All Sky Survey, which is a joint project of the University of Massachusetts and the Infrared Processing and Analysis Center, funded by the National Aeronautics and Space Administration and the National Science Foundation. The Nançay Radio Observatory, which is the Unité Scientifique de Nançay of the Observatoire de Paris, is associated with the French Centre National de Recherche Scientifique (CNRS) as USR B704, and acknowledges the financial support of the Région Centre as well as of the European Union. This research also has made use of the Lyon-Meudon Extragalactic Database (LEDA), recently incorporated in HyperLeda, the NASA/IPAC Extragalactic Database (NED) which is operated by the Jet Propulsion Laboratory, California Institute of Technology, under contract with the National Aeronautics and Space Administration

Table 2. Comparison with published H I data.

No.	PGC	Ident.	V_{HI} km s^{-1}	W_{50} km s^{-1}	I_{HI} Jy km s^{-1}	Tel.	Ref.
Clearly detected galaxies							
L6O	0930	NGC 45	467	156	66.2	N	this paper
			474		–	G43	Haynes & Roberts (1979)
			461	–	–	IAR	Bajaja (1979)
			468	–	–	P	Reif et al. (1982)
			470	–	211	E	Huchtmeier et al. (1981)
			470	172	217	O	Rogstad et al. (1967)
			467	165	–	J	Dean & Davies (1975)
			471	—	227	G43	Fisher & Tully (1975)
			471	174	238	G43	Fisher & Tully (1981)
			468	167	242	E	Huchtmeier & Seiradakis (1985)
			459	–	384	P	Lewis (1972)
L53O	4650	UGC 825	5334	289	2.5	N	this paper
			5338	292	2.7	N	Matthews & van Driel (2000)
L57O*	4734	UGC 847	5240	266	2.4	N	this paper
			5238	265	2.7	G	Haynes & Giovanelli (1991)
L99O	8078	UGC 1601	5567	225	5.7	N	this paper
			5591	260	6.9	E	Haynes et al. (1999)
L117O*	9431	NGC 948	4755	165	2.7	N	this paper
			4487	181	6.0	G43	Haynes et al. (1999)
L125O*	9831	NGC 980	5733	582	4.0	N	this paper
			5757	–	8.1	G	Magri (1994)
			5737	702	8.2	G	Haynes et al. (1988)
L182O	12664	MCG -2-9-36	2801	215	15.2	N	this paper
			2808	222	18.4	G	Fisher & Tully (1981)
			2806	–	19.4	G	Tifft & Cocke (1988)
L336O	23319	UGC 4329	4096	218	6.8	N	this paper
			4092	–	7.8	A	Schombert et al. (1981)
			4098	224	–	A	Lewis (1983)
			4090	232	7.5	A	Bothun et al. (1985)
			4098	243	7.0	A	Lewis et al. (1985)
			4095	221	8.2	A	Bicay & Giovanelli (1986)
			4100	–	8.4	G	Tifft & Cocke (1988)
			4106	212	6.0	A	Rosenberg & Schneider (2000)
L345O*	23977	ESO 495-17	1476	201	3.2	N	this paper
			1467	179	3.7	N	Chamaraux et al. (1999)
L352O	24489	ESO 563-16	1732	184	16.4	N	this paper
			1732	180	16.6	N	Fouqué et al. (1990)
L360O*	25281	NGC 2719	3077	211	9.3	N	this paper
			3157	203	15.7	A	Bicay & Giovanelli (1986)
			3167	–	16.7	G	Davis & Seaquist (1983)
L364O	25472	UGC 4753	1828	159	2.1	N	this paper
			1851	172	3.9	N	Matthews & van Driel (2000)
L371O*	26238	NGC 2799	1673	156	9.1	N	this paper
			1755	343	11.1	N	Bottinelli et al. (1982)
			1750	304	10.9	N	van Driel et al. (2001)
L430O	32204	UGC 5879	5612	278	5.5	N	this paper
			5612	283	5.4	N	Matthews & van Driel (2000)
L4450	33860	IC 2627	2087	50	10.8	N	this paper
			2075	34	18.4		Davies (1980)
			2090	40	24.2	E	Fisher & Tully (1981)
			2082	39	24.8	E	Richter & Huchtmeier (1987)
			2075	–	21.9	P	Reif et al. (1982)
L447O	34497	UGC 6307	1906	207	7.5	N	this paper
			1964	206	5.2	G	Schneider et al. (1992)
L455O	35292	NGC 3691	987	125	2.9	N	this paper
			1067	125	2.6	A	Helou et al. (1982)
			1071	145	4.0	A	Giovanardi & Salpeter (1985)
			1080	128	3.1	A	Lewis et al. (1985)
			1113	–	5.0	G	Tifft & Cocke (1988)
L487O	37914	UGC 7000	1492	80	6.1	N	this paper
			1483	67	5.7	A	Sulentic & Arp (1983)
			1487	75	5.5	A	Schneider et al. (1986)
			1498	79	5.9	A	Schneider et al. (1986)
			1487	–	7.52	G	Richter & Huchtmeier (1987)
			1475	–	21.1	A	Impey et al. (1996)

Table 2. continued.

No.	PGC	Ident.	V_{HI} km s^{-1}	W_{50} km s^{-1}	I_{HI} Jy km s^{-1}	Tel.	Ref.
Clearly detected galaxies – continued							
L497O	38897	NGC 4173	1120	160	27.6	N	this paper
			1127	170	42.1	G	Fisher & Tully (1981)
			1085	80	19.8	A	Bothun et al. (1985)
			1127	–	–	E	Garcia-Baretto et al. (1994)
			1096	164	34.2	N	Kraan-Korteweg et al. (1999)
L512O	40092	IC 784	4872	387	9.2	N	this paper
			4865	–	11.0	G	Richter & Huchtmeier (1987)
			4876	–	6.2	N	Paturel et al. (2003)
L572O	46664	NGC 5105	2902	214	9.9	N	this paper
			2904	–	14.95	G	Richter & Huchtmeier (1987)
			2903	215	14.52	G	Haynes et al. (1999)
F38O	48621	UGC 8688	1359	60	5.0	N	this paper
			1355	63	5.4	E	Huchtmeier et al. (2000)
L634O	52012	CGCG 133-87	4782	230	4.7	N	this paper
			4781	259	5.9	A	Mould et al. (1993)
			4783	–	2.8	A	Freudling (1995)
L639O	52612	ESO 580-14	6080	96	3.3	N	this paper
			6080	82	3.1	N	Fouqué et al. (1990)
L643O	52853	MCG-2-38-15	1979	217	22.3	N	this paper
			2045	200	23.4	G	Thonnard et al. (1978)
			2046	–	–	N	Theureau et al. (1998)
L735O	63425	ESO 594-8	6136	325	4.4	N	this paper
			6140	345	6.0	G	Haynes et al. (1999)
L746O	64448	ESO 462-7	6130	323	6.9	N	this paper
			6132	331	8.7	N	Haynes et al. (1999)
L752O	91678	FGC 2286	3783	245	3.7	N	this paper
			3825	256	3.2	N	Matthews & van Driel (2000)
L781O	68645	UGC 11999	3287	162	2.0	N	this paper
			3298	174	2.5	N	Matthews & van Driel (2000)
L788O	68996	IC 1447	2953	315	3.7	N	this paper
			2967	291	4.8	N	Theureau et al. (1998)
Marginally detected galaxies							
L739O	63776	ESO 526-11	5855	292	2.5	N	this paper
			5844	300	1.9	N	Paturel et al. (2003)
			5855	294	2.5	N	Haynes et al. (1999)
Undetected galaxies							
L180O	12439	FGC 410	–	–	<4.0	N	this paper
			2756	236	3.0	N	Matthews & van Driel (2000)
L467O	36381	UGC 6679	–	–	<2.5	N	this paper
			5172	326	2.8	N	Matthews & van Driel (2000)
L630O	51628	ESO 447-5	–	–	<3.6	N	this paper
			7128	273	3.2	N	Matthews & van Driel (2000)
L673O	57278	MCG 3-41-136	–	–	<2.3	N	this paper
			10596	452	1.2	A	Bothun et al. (1985)
			10627	452	1.6	A	Haynes et al. (1997)

Note: a "*" following a name in Col. 1 indicates a confused spectrum, see Sect. 4.5.
Telescope codes:
A: Arecibo 305-m; E: Effelsberg 100-m; G: Green Bank 90-m; G43: Green Bank 43-m; IAR: I.A.R. 30-m; J: Jodrell Bank 76-m; N: Nançay 94-m equiv; O: Owens Valley; P: Parkes 64-m.

and the Aladin database, operated at CDS, Strasbourg, France. We acknowledge financial support from CNRS/NSF collaboration grant No. 10637.

References

Allen, C. W. 1973, Astrophysical Quantities (London: Athlone Press)
Bajaja, E. 1979, Pub. Univ. Chile, 3, 64
Balkowski, C. 1979, A&A, 78, 190
Bergvall, N., Rönnback, J., Masegosa, J., & Östlin, G. 1999, A&A, 341, 697
Bicay, M. D., & Giovanelli, R. 1986, AJ, 91, 732
Blackman, C. P. 1980, MNRAS, 191, 123
Boissier, N., Prantzos, N., Monnier Ragaigne, D., et al. 2003, MNRAS, in press [astro-ph/0304313]
Boselli, A., Gavazzi, G., Franzetti, P., Pierini, D., & Scodeggio, M. 2000, A&A, 142, 73
Bothun, G. D., Aaronson, M., Schommer, R. A., et al. 1985, ApJS, 57, 423
Bothun, G. D., Impey, C. D., Malin, D. F., & Mould, J. R. 1987, AJ, 94, 23
Bottinelli, L., Gouguenheim, L., & Paturel, G. 1980, A&A, 88, 32
Bottinelli, L., Gouguenheim, L., & Paturel, G. 1982, A&A, 113, 61
Bottinelli, L., Gouguenheim, L., Theureau, G., Coudreau, N., & Paturel, G. 1999, A&AS, 135, 429
Chamaraux, P., Masnoux, J. L., Kazes, I., et al. 1999, MNRAS, 307, 236
Chung, A., van Gorkom, J. H., O'Neil, K., & Bothun, G. D. 2002, AJ, 123, 2387
da Costa, L. N., Willmer, C. N. A., Pellegrini, P. S., et al. 1998, AJ, 116, 1
Davies, R. D. 1980, private communication
Davis, L. E., & Seaquist, E. R. 1983, ApJS, 53, 269
Dean, J. F., & Davies, R. D. 1975, MNRAS, 170, 503

de Vaucouleurs, G., de Vaucouleurs, A., Corwin, H. G., et al. 1991, The Third Reference Catalogue of Bright Galaxies (New York: Springer-Verlag) (RC3)
Fisher, J. R., & Tully, R. B. 1975, ApJS, 44, 151
Fisher, J. R., & Tully, R. B. 1981, ApJS, 47, 139
Freudling, W. 1995, A&AS, 112, 429
Fridman, P. A., & Baan, W. A. 2001, A&A, 378, 327
Fouqué, P., Bottinelli, L., Durand, N., Gouguenheim, L., & Paturel, G. 1990, A&AS, 86, 473
Garcia-Baretto, J. A., Downes, D., & Huchtmeier, W. K. 1994, A&A, 288, 705
Giovanardi, C., & Salpeter, E. E. 1985, ApJS, 58, 623
Grogin, N. A., & Geller, M. J. 2000, AJ, 119, 32
Haynes, M. P., Giovanelli, R., Starosta, B. M., & Magri, C. 1988, AJ, 95, 607
Haynes, M. P., & Roberts, M. S. 1979, ApJ, 227, 767
Haynes, M. P., & Giovanelli, R. 1991, A&AS, 77, 331
Haynes, M. P., Giovanelli, R., Herter, T., et al. 1997, AJ, 113, 1197
Haynes, M. P., Giovanelli, R., Chamaraux, P., et al. 1999, AJ, 117, 2039
ITU-R Radio Regulations 2001, International Telecommunication Union (Geneva, Switzerland)
Helou, G., Salpeter, E. E., & Terzian, Y. 1982, AJ, 87, 1443
Huchra, J. H., Latham, D. W., da Costa, L. N., et al. 1993, AJ, 105, 1637
Huchtmeier, W. K., Seiradakis, J. H., & Materne, J. 1981, A&A, 102, 134
Huchtmeier, W. K. 1982, A&A, 110, 121
Huchtmeier, W. K., & Seiradakis, J. H. 1985, A&A, 143, 216
Huchtmeier, W. K., Karachentsev, I. D., Karachentseva, V. E., & Ehle, M. 2000, A&AS, 141, 469
Hurt, R. L., Jarrett, T. H., Kirkpatrick, J. D., et al. 2000, AJ, 120, 1876
Impey, C. D., Sprayberry, D., Irwin, J. A., & Bothun, G. D. 1996, ApJS, 105, 209
Jarrett, T. H., Chester, T., Cutri, R., et al. 2000a, AJ, 119, 2498
Jarrett, T. H., Chester, T., Cutri, R., et al. 2000b, AJ, 120, 298
Kraan-Korteweg, R. C., van Driel, W., Briggs, F., Binggeli, B., & Mostefaoui, T. I. 1999, A&AS, 135, 255
Lewis, B. M. 1972, Aust. J. Phys., 25, 315
Lewis, B. M. 1983, AJ, 88, 962
Lewis, B. M., Helou, G., & Salpeter, E. E. 1985, ApJS, 59, 161
Magri, C. 1994, AJ, 108, 896
Mathewson, D. S., & Ford, V. L. 1996, ApJS, 107, 97
Matthews, L. D., & van Driel, W. 2000, A&A, 143, 421
Matthews, L. D., van Driel, W., & Monnier-Ragaigne, D. 2001, A&A, 365, 1
McGaugh, S. S., & de Blok, W. J. G. 1997, ApJ, 481, 689
McGaugh, S. S., Rubin, V. C., & de Blok, W. J. G. 2001, AJ, 122, 2381
Monnier Ragaigne, D., van Driel, W., Schneider, S. E., Jarrett, T. H., & Balkowski, C. 2003a, A&A, 405, 99 (Paper I)
Monnier Ragaigne, D., van Driel, W., Schneider, S. E., et al. 2003b, A&A, 408, 67 (Paper II)
Monnier Ragaigne, D., Papaderos, P., van Driel, W., et al. 2003d, A&A, in preparation (Paper IV)
Mould, J. R., Akeson, R. L., Bothun, G. D., et al. 1993, ApJ, 409, 14
O'Neil, K., Bothun, G. D., & Cornell, M. E. 1997a, AJ, 113, 1212
O'Neil, K., Bothun, G. D., Schombert, J., Cornell, M. E., & Impey, C. D. 1997b, AJ, 114, 2448
O'Neil, K., Bothun, G. D., & Schombert, J. 2000, AJ, 119, 136
Paturel, G., Bottinelli, L., Di Nella, H., et al. 1997, A&AS, 124, 109
Paturel, G., Theureau, G., Bottinelli, L., et al. 2003, A&A, in preparation
Peterson, S. D., & Shostak, G. S. 1974, AJ, 79, 767
Reif, K., Mebold, U., Goss, W. M., van Woerden, H., & Siegman, B. 1982, A&AS, 50, 451
Rhee, G., & van Albada, T. S. 1996, A&AS, 115, 407
Richter, O.-G., & Huchtmeier W. K. 1987, A&AS, 68, 427
Rogstad, D. H., Rougoor, G. W., & Whiteoak, J. B. 1967, ApJ, 150, 9
Rosenberg, J. L., & Schneider, S. E. 2000, ApJS, 130, 177
Schneider, S. E., Helou, G., Salpeter, E. E., & Terzian, Y. 1986, AJ, 92, 742
Schneider, S. E., Thuan, T. X., Mangum, J. G., & Miller, J. 1992, ApJS, 81, 5
Schneider, S, Huchra, J., Jarrett, T., & Chester, T. 1997, 2MASS Extragalactic Studies: Early Results from the Prototype Camera, in The Impact of Large-Scale Near-IR Sky Surveys, ed. F. Garzon, et al. (Dordrecht: Kluwer), 231
Schommer, R. A., Sullivan III, W. T., & Bothun, G. D. 1981, AJ, 86, 943
Shostak, G. S. 1978, A&A, 68, 321
Spitzak, J. G., & Schneider, S. E. 1998, ApJS, 119, 159
Staveley-Smith, L., & Davies, R. D. 1987, MNRAS, 224, 953
Sulentic, J. W., & Arp, H. 1983, AJ, 88, 489
Theureau, G., Bottinelli, L., Coudreau-Durand, N., et al. 1998, A&AS, 130, 333
Thonnard, N., Rubin, V. C., Ford, Jr. W. K., & Roberts, M. S. 1978, AJ, 83, 1564
Tifft, W. G., & Cocke, W. J. 1988, ApJS, 67, 1
van den Hoek, L. B., de Blok, W. J. G., van der Hulst, J. M., & deJong, T. 2000, A&A, 357, 397
van Driel, W., Pezzani, J., & Gérard, E. 1997, Renovating the Nançay radio telescope: the FORT project, in High-sensitivity Radio Astronomy, ed. N. Jackson, & R. J. Davies (Cambridge: Cambridge Univ. Press), 229
van Driel, W., Arnaboldi, M., Combes, F., & Sparke, L. S. 2000, A&AS, 141, 385
van Driel, W., Marcum, P., Gallagher III, J. S., et al. 2001, A&A, 378, 370
van der Hulst, J. M., Skillman, E. D., Smith, T. R., et al. 1993, AJ, 106, 548
van Zee, L., Haynes, M. P., & Salzer, J. J. 1997, Star Formation Activity in High M/L Galaxies, in Dwarf Galaxies: Probes for galaxy formation and Evolution, Joint Discussion, Kyoto, Japan, 14
Verheijen, M. A. W., & Sancisi, R. 2001, A&A, 370, 765

Online Material

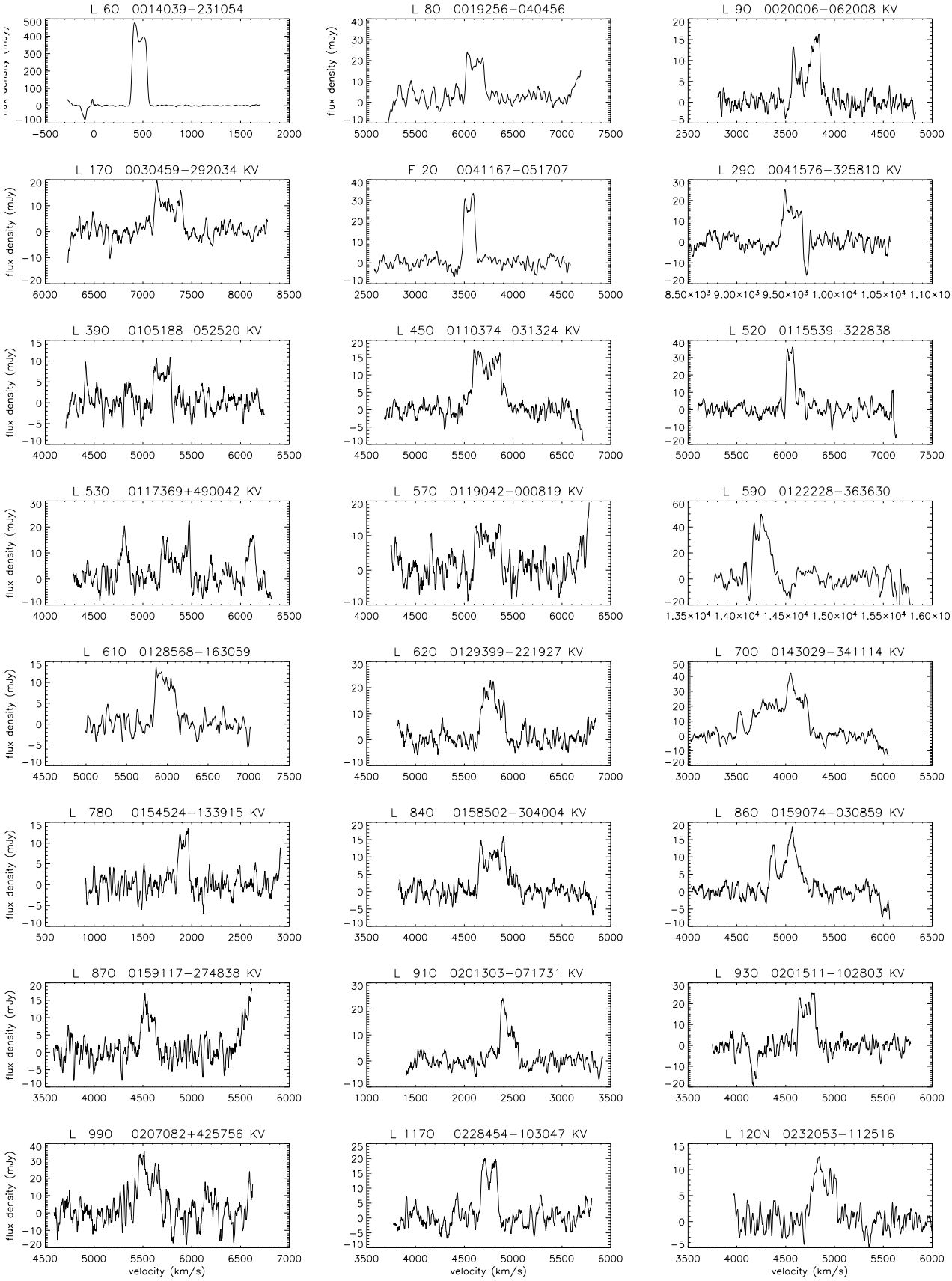

Fig. 1. a) Nançay 21-cm H I line spectra of detected objects (see Table 3). Velocity resolution is 15.8 km s^{-1} (velocity search mode) and 17.1 km s^{-1} (known velocity mode), radial heliocentric velocities are according to the optical convention. Galaxies detected in the "known velocity" mode are indicated by the designation "KV" following their coordinates in the header of their spectrum.

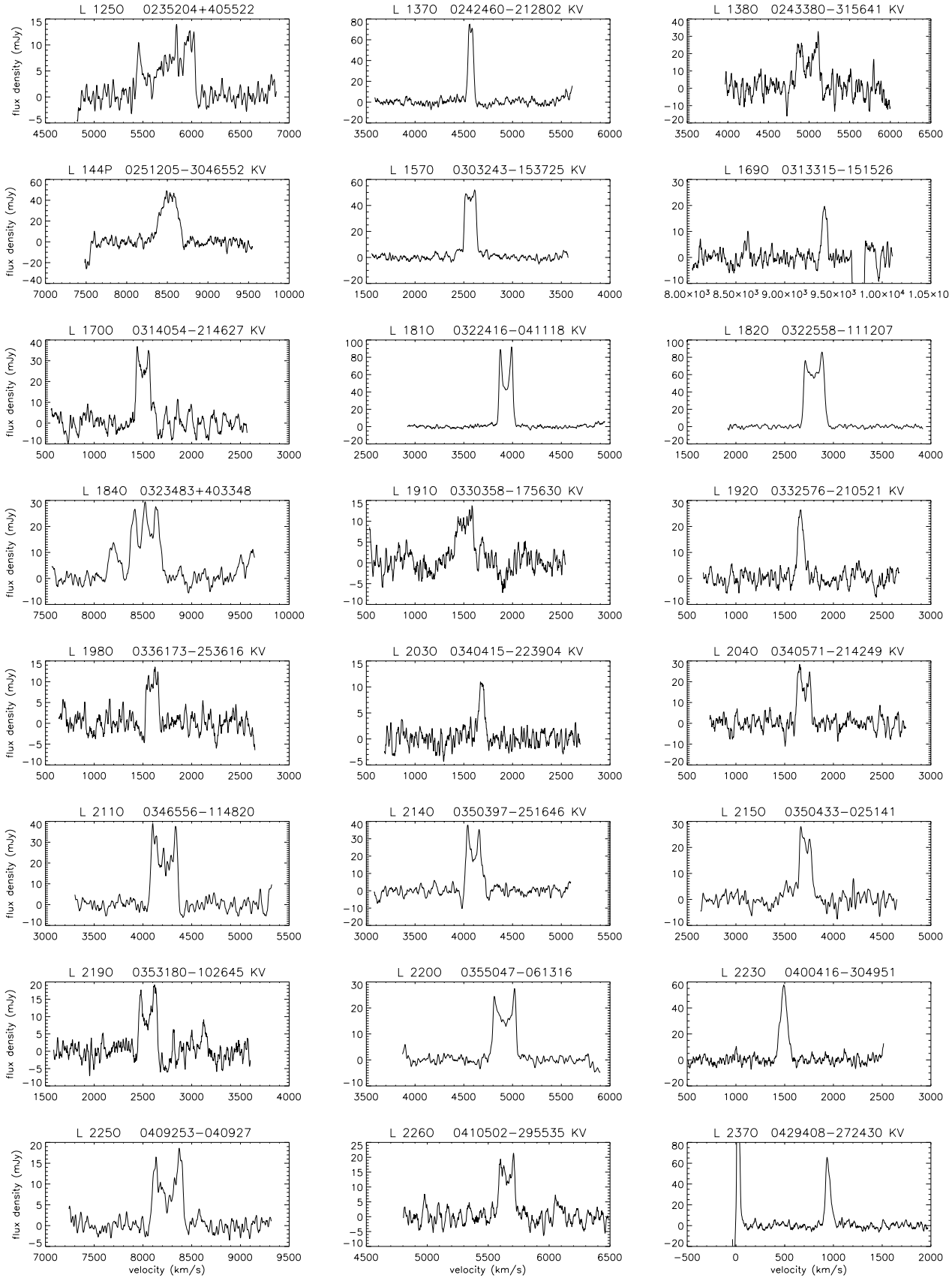

Fig. 1. b) continued.

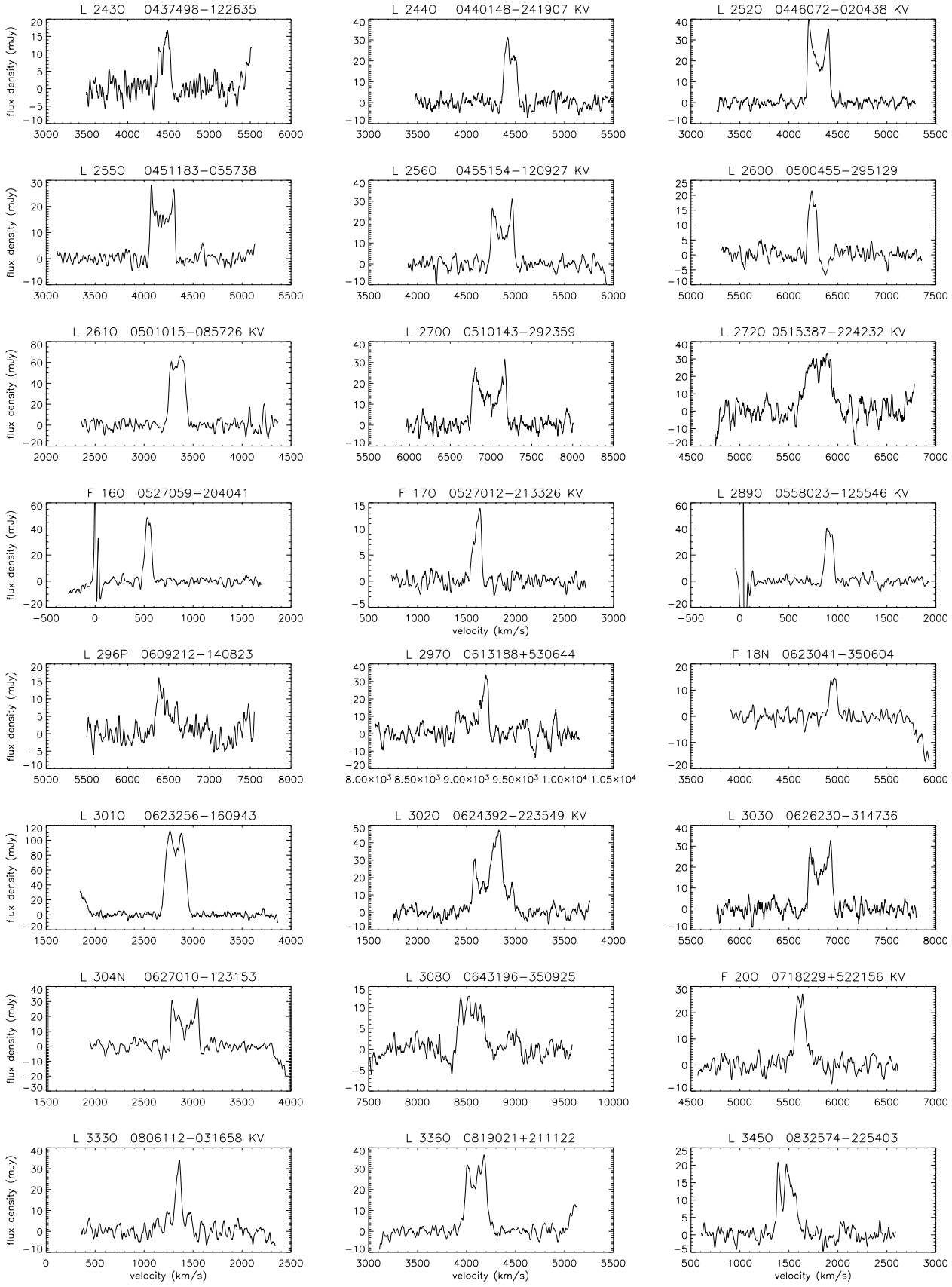

Fig. 1. c) continued.

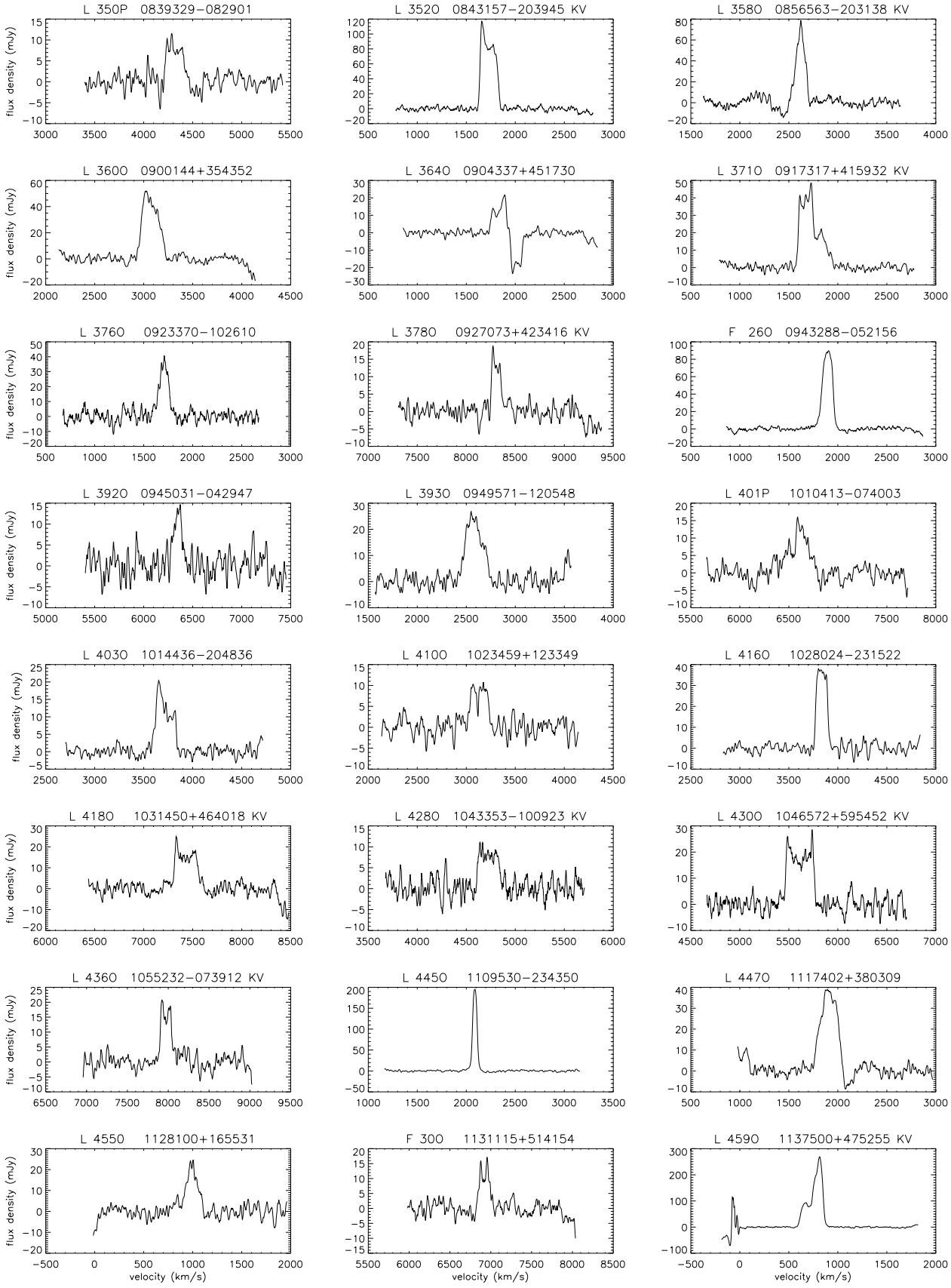

Fig. 1. d) continued.

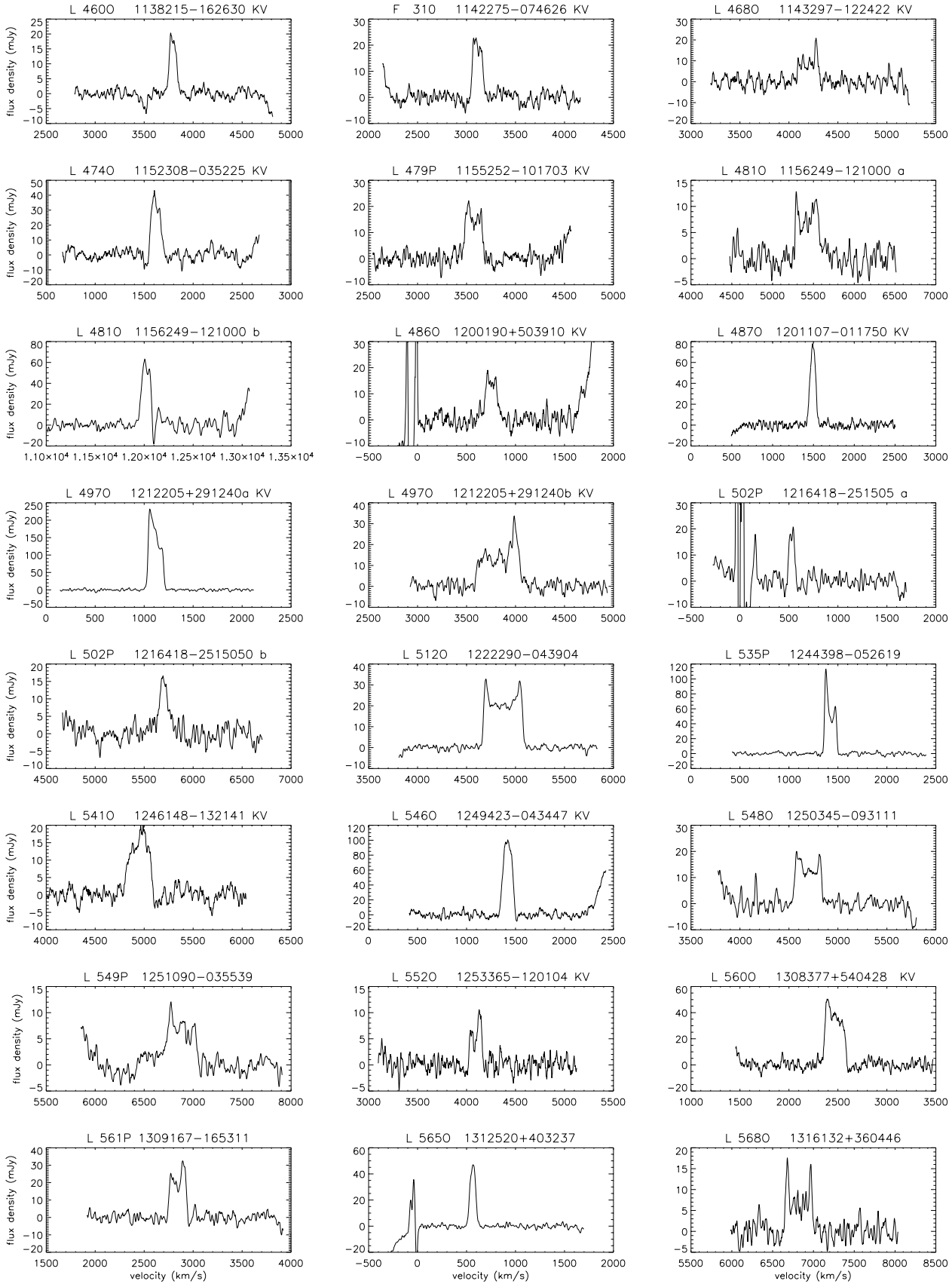

Fig. 1. e) continued.

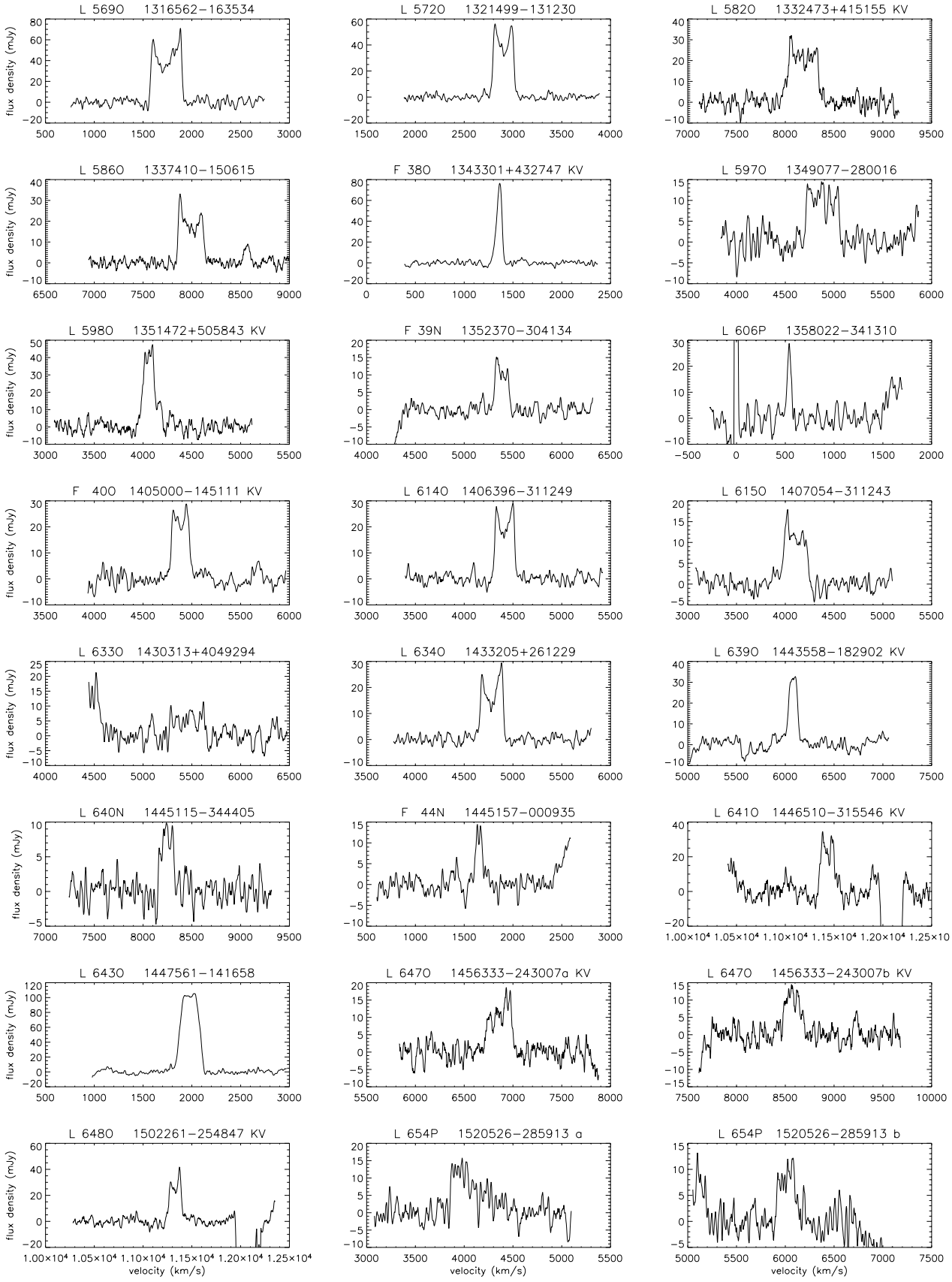

Fig. 1. f) continued.

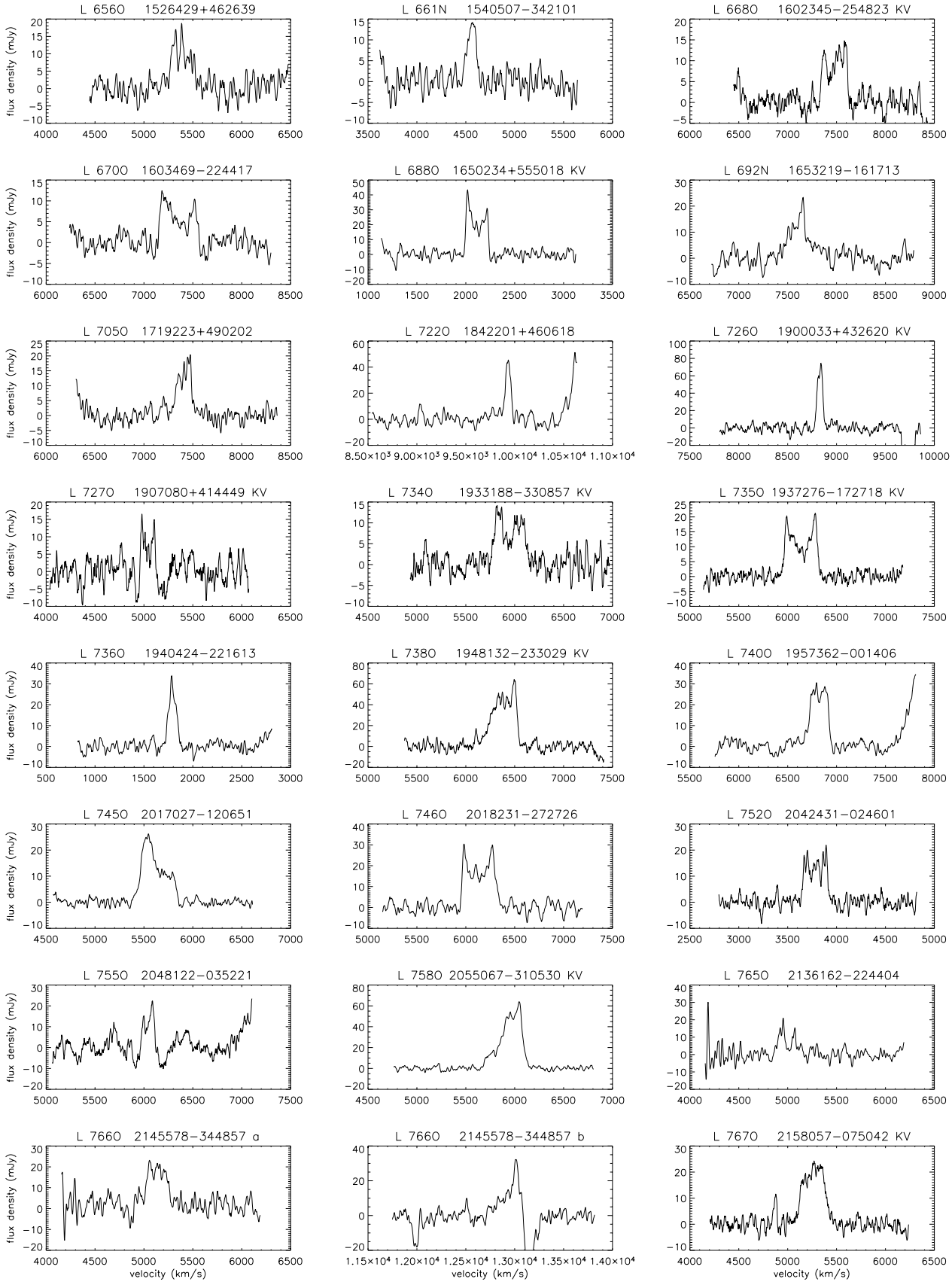

Fig. 1. g) continued.

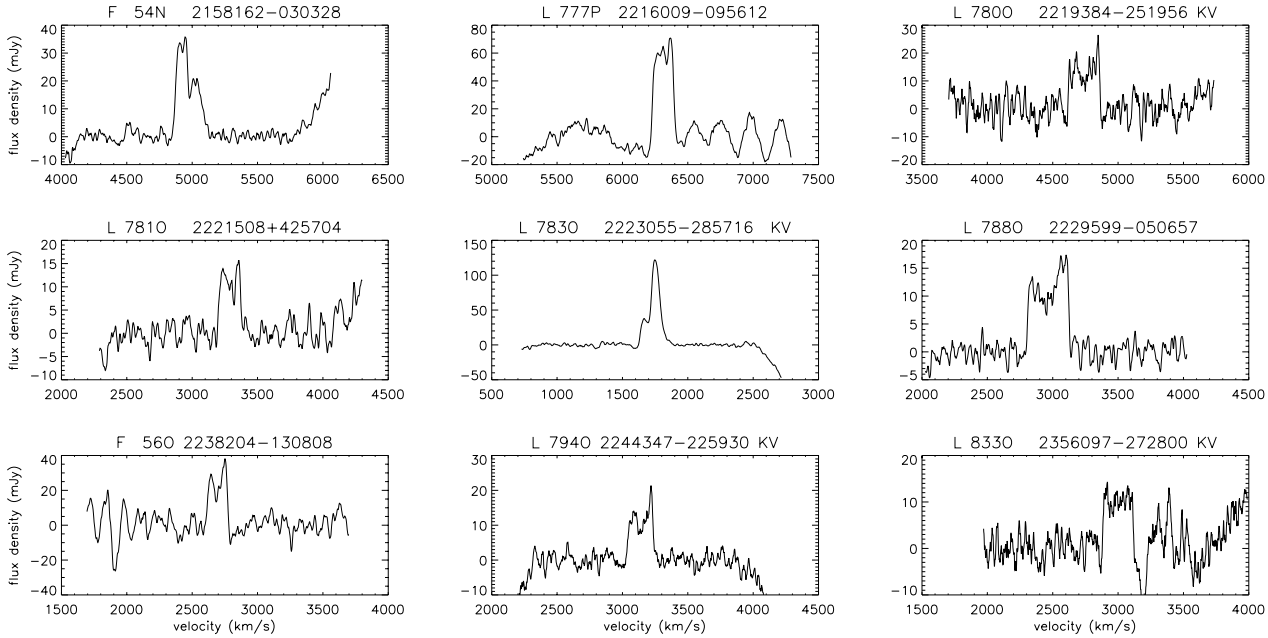

Fig. 1. h) continued.

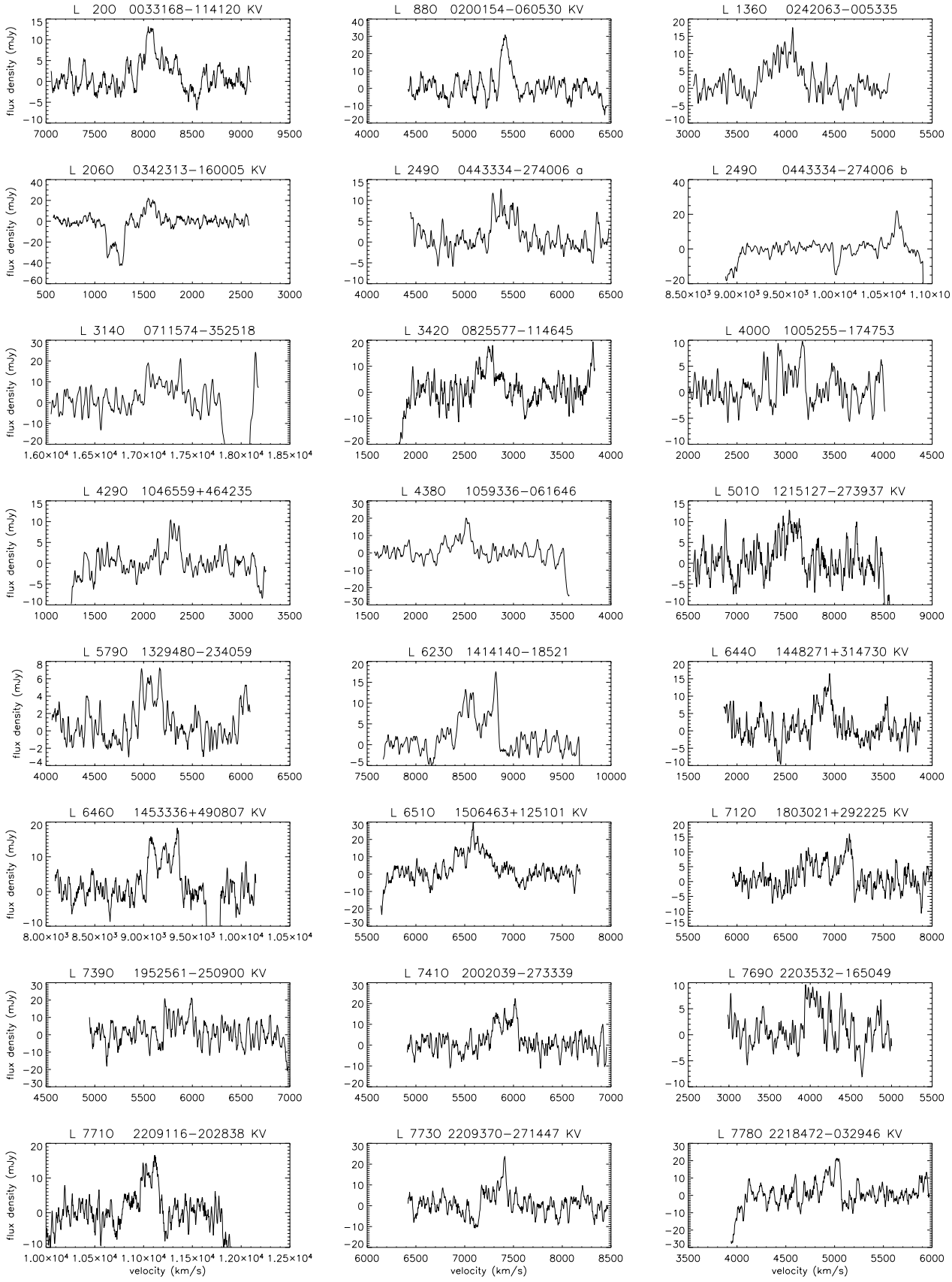

Fig. 2. a) Nançay 21-cm H I line spectra of marginal detections (see Table 4). Velocity resolution is 15.8 km s^{-1} (velocity search mode) and 17.1 km s^{-1} (known velocity mode), radial heliocentric velocities are according to the optical convention. Galaxies detected in the "known velocity" mode are indicated by the designation "KV" following their coordinates in the header of their spectrum.